東京大学大学院新領域創成科学研究科
基盤科学研究系
先端エネルギー工学専攻

２０００年度修士論文

Relaxed states in solar corona and high-beta plasmas

– Double Beltrami fields –

太陽コロナ、高ベータプラズマにおける緩和状態

– 二重 Beltrami 平衡 –

学籍番号　９６２０１
氏名　大崎 秀一
指導教官　吉田 善章 教授

（２００１年2月１３日提出）

Contents

Chapter 1

Introduction

Beltrami fields, eigenfunctions of the curl operator, represent essential characteristics of sheared, spiral, chiral or helical structures in various vector fields. The Beltrami condition that demands the alignment of a vorticity with its flow describes the simplest and perhaps the most fundamental equilibrium state in a vortex dynamic system. The resulting Beltrami fields constitute a null set for the generator of the evolution equation describing the vortex dynamics. It is also believed that the Beltrami fields are accessible and robust in the sense that they emerge as the nonlinear dynamics of vortices tends to self-organize the system through a weakly dissipative process [1, 2].

A general solenoidal (divergence-free) vector field, such as a magnetic field

or an incompressible flow, can be decomposed into an orthogonal sum of the Beltrami fields [3, 4]. Nonlinear dynamics of plasmas induce complex couplings among these Beltrami fields. In a single-fluid MHD plasma, however, the relaxed state is expressed by a single Beltrami magnetic field, resulting in the self-organization of a force-free equilibrium, which is the Taylor relaxed state [5]. The Beltrami magnetic fields are studied and observed in different plasma systems of space and laboratory [6]-[14].

In a two-fluid MHD plasma, by relating the velocity and the magnetic fields, a more general relaxed state is given by a double Beltrami field that is expressed by the superposition of two different Beltrami fields [15, 16]. The double Beltrami fields, where velocity and magnetic fields are strongly coupled, include field structures far richer than the conventional single Beltrami fields. This new set of relaxed states, despite its simple mathematical structure, can express a variety of plasma states and explain interesting phenomena. Furthermore, it is shown that a generalized Bernoulli condition is satisfied simultaneously with the Beltrami condition. As the generalized Bernoulli conditions describe homogeneous distributions of the energy density, the Beltrami-Bernoulli states may follow from the concept of relaxed states. In the two-fluid MHD, the Beltrami-Bernoulli condition predicts the possibility of producing a very high-

beta equilibrium, which is not allowed in the single Beltrami states. The double Beltrami field can be classified as a relaxed state that has a more complicated structure (higher energy) than the single Beltrami field. A general theory of the Beltrami field as relaxed state and a theory of the double Beltrami field are given in Chap. 2.

Plasma flows have been observed and attracted huge attention in space plasmas. For example, in the solar corona, the TRACE (Transition Region and Coronal Explorer) observations have recently revealed that the corona is comprised of lots of thin loops that are intrinsically dynamic and full of flows [17]-[20]. At present, many researchers already pay attention to the plasma flow in the solar corona and there are several publications cataloging enough observational evidence for flows in the regions between the sun and the corona [17]-[28].

On the other hand, in the many experimental studies of magnetically confined plasmas over several decades, one of the less appreciated phenomena has been flow, that is, until recent years. Thus, it appears that significant flows are common feature of magnetic plasmas. Further, various favorable effects have been attributed to flows, including the stabilization of ballooning modes by sheared flow, and reduced transport rate (H-mode). Theoretical studies

of equilibria of flowing plasmas date to the 1950s, but most have been from mid-1970s ([29, 30] and the references therein).

In this thesis, first, we note that the double Beltrami field, which is a relaxed state coupling the magnetic field and the flow, can include far rich field configurations in spite of its simple mathematical structure. Then, in Chap. 3, an algebraic structure of the double Beltrami field is discussed and we give an attempt to explain the trigger of solar eruptive events. The double Beltrami field is characterized by four parameters (two eigenvalues and two amplitudes). In relating these parameters with macroscopic constants of motion (two helicities and energy), an interesting set of algebraic relations is derived. Using these relations, we observe that, when macroscale of interacting loop structures decreases sharply on condition that the energy is larger than some critical value, a fold catastrophe appears and an equilibrium is lost. Applying this model to the solar corona, it is shown that magnetic field energy transfer to flow is possible and solar eruptive events (flares, prominences, CMEs - coronal mass ejections) may happen.

Next, we pay attention to a high-beta equilibrium of the double Beltrami field. The Beltrami-Bernoulli condition predicts that, when the flow velocity is comparable to the Alfvén speed, a high-beta equilibrium can be produced

in which the plasma pressure is primarily balanced by the dynamic pressure of the flow. To obtain such a fast flow in plasmas, a nonneutral condition is proposed, which can actually produce a self-electric field $\boldsymbol{E}$ in plasmas, causing strong $\boldsymbol{E} \times \boldsymbol{B}$ shear flow if we apply an appropriate magnetic field $\boldsymbol{B}$ there. For this purpose, a new method of toroidal non-neutral plasma trap has been developed using a proto-type device "Proto-RT" [31]. At the same time, theoretical studies on flowing toroidal equilibria are progressing too [32, 33]. In Chap. 4, we discuss a high-beta toroidal equilibrium of the double Beltrami states and present a numerical solution. Using a Clebsch representation to the magnetic and the velocity field, the double Beltrami equation translates as a coupled Grad-Shafranov equation, which can be solved numerically. Further, we discuss a shock formation in this equilibrium, using the conventional MHD shock condition (evolutionary condition).

Summary is given in Cap. 5.

Chapter 2

Beltrami condition and relaxed state – Double Beltrami fields

2.1 General vortex dynamics and Beltrami condition

We start with reviewing the prototype equation for vortex dynamics. Let $\boldsymbol{\omega}$ be a three dimensional vector field representing a certain vorticity in $\boldsymbol{R}^3$. We consider an incompressible flow $\boldsymbol{U}$ that transports $\boldsymbol{\omega}$. When the circulation associated with the vorticity is conserved everywhere, this $\boldsymbol{\omega}$ obeys the equa-

tion

$$\frac{\partial}{\partial t}\boldsymbol{\omega} - \nabla \times (\boldsymbol{U} \times \boldsymbol{\omega}) = 0. \tag{2.1}$$

The general steady states of (2.1) are given by

$$\boldsymbol{U} \times \boldsymbol{\omega} = \nabla\varphi, \tag{2.2}$$

where φ is a certain scalar field, which physically corresponds to the energy density (pressure) in the original (decurled) equation.

The Beltrami condition, which demands alignment of vortices and flows, is expressed by

$$\boldsymbol{\omega} = \mu\boldsymbol{U}, \tag{2.3}$$

where μ is a certain scalar function. The Beltrami condition (2.3), thus, gives a special class of solution such that

$$\boldsymbol{U} \times \boldsymbol{\omega} = 0 = \nabla\varphi. \tag{2.4}$$

The former equality is the Beltrami condition, while the latter, demanding that the energy density is homogeneous, is a "generalized Bernoulli condition".

We note that the constancy of the energy density refers to the direction perpendicular, as well as parallel, to the stream line $\boldsymbol{U}$. This is an essential difference from the conventional Bernoulli condition. It might appear that

the Beltrami-Bernoulli states are very special and may be inaccessible. These conditions, however, follow from the concept of relaxed states. Indeed, the generalized Bernoulli condition describes homogeneous distributions of the energy density. Therefore, it is believed that the Beltrami fields are accessible and robust in the sense that they emerge as the nonlinear dynamics of vortices tends to self-organize the system through a weakly dissipative process [1, 2], [34].

The simplest example of the vortex dynamics equation is that of the Euler equation of incompressible ideal flows. Let $\boldsymbol{U}$ be an incompressible flow that obeys

$$\frac{\partial}{\partial t}\boldsymbol{U} + (\boldsymbol{U}\cdot\nabla)\boldsymbol{U} = -\nabla p, \tag{2.5}$$

where p is the pressure. Taking the curl of (2.5), we obtain the evolution equation for the vorticity $\boldsymbol{\omega} = \nabla\times\boldsymbol{U}$, which reads as (2.1). Then the Beltrami flow is expressed by

$$\nabla\times\boldsymbol{U} = \mu\boldsymbol{U}. \tag{2.6}$$

We note that (2.6) is not Galilei-transform invariant. We thus consider a bounded domain and impose a boundary condition to remove the freedom of the Galilei transform. Taking the divergence of (2.6), we find that the scalar

function μ must satisfy

$$\boldsymbol{U} \cdot \nabla \mu = 0, \tag{2.7}$$

demanding that μ must remain constant along each streamline of the flow $\boldsymbol{U}$. An analysis of the nonlinear system of elliptic-hyperbolic partial differential equations (2.6)-(2.7) involves extremely difficult mathematical issues. The characteristic curve of (2.7) is the streamline of the unknown flow $\boldsymbol{U}$, which can be chaotic (nonintegrable) in general three-dimensional problems. Two special cases, however, can be studied rigorously. One is the case where $\boldsymbol{U}$ has a coordinate that one can ignore (two-dimensional). Then, the streamline equation becomes integrable, and the system (2.6)-(2.7) reduces into a nonlinear elliptic equation [1, 35]. The other one is the case where μ is a constant number. It makes (2.7) trivial and the analysis reduces into a simple but nontrivial problem, i.e., the eigenvalue problem of the curl operator [3].

We end this section by reviewing another example of vortex dynamics; the magnetohydrodynamic (one-fluid MHD) description of a plasma. The two principal equations of the ideal (dissipation-less) conducting-fluid model are

$$\boldsymbol{E} + \boldsymbol{U} \times \boldsymbol{B} = 0, \tag{2.8}$$

$$\frac{\partial}{\partial t}\boldsymbol{U} + (\boldsymbol{U} \cdot \nabla)\boldsymbol{U} = \frac{1}{\rho}\left(\boldsymbol{j} \times \boldsymbol{B} - \nabla p\right), \tag{2.9}$$

where $\boldsymbol{U}$, $\boldsymbol{j}$, $\boldsymbol{E}$ and $\boldsymbol{B}$ are, respectively, the flow velocity, the current density, the electric field and the magnetic field measured in a certain fixed coordinates, and ρ is the fluid mass density that is assumed to be constant. Using Faraday's law

$$\frac{\partial \boldsymbol{B}}{\partial t} = -\nabla \times \boldsymbol{E}, \tag{2.10}$$

and taking the curl of (2.8) and (2.9), we obtain

$$\frac{\partial}{\partial t}\boldsymbol{B} - \nabla \times (\boldsymbol{U} \times \boldsymbol{B}) = 0, \tag{2.11}$$

$$\frac{\partial}{\partial t}\boldsymbol{\omega} - \nabla \times \left(\frac{\boldsymbol{j} \times \boldsymbol{B}}{\rho} + \boldsymbol{U} \times \boldsymbol{\omega} \right) = 0, \tag{2.12}$$

where $\boldsymbol{\omega} = \nabla \times \boldsymbol{U}$. The Beltrami conditions for this system of vortex dynamics equations are

$$\boldsymbol{j} = \mu_1 \boldsymbol{B} = \mu_2 \boldsymbol{U} = \mu_3 \boldsymbol{\omega}. \tag{2.13}$$

Using the expression $\boldsymbol{j} = \nabla \times \boldsymbol{B}/\mu_0$ in the first equality of (2.13), we get

$$\nabla \times \boldsymbol{B} = \mu \boldsymbol{B}, \tag{2.14}$$

which implies that $\boldsymbol{B}$ parallels its own vorticity [cf. (2.6)]. This configuration, for which the magnetic stress $\boldsymbol{j} \times \boldsymbol{B}$ vanishes, is aptly called "force-free".

In order to characterize the stellar magnetic fields, solutions to (2.14) were intensively studied in 1950s [6] - [8]. For $\mu \neq 0$, the magnetic field $\boldsymbol{B}$ has a

finite curl, and hence, the field lines are twisted. The current (proportional to $\nabla \times \boldsymbol{B}$), flowing parallel to the twisted field lines, creates what may be termed as "paramagnetic" structures. Such twisted magnetic field lines appear commonly in many different plasma systems such as the magnetic ropes created in solar and geo-magnetic systems [9], and galactic jets [10]. Solar flares and coronal mass ejections (CMEs) creates magnetic clouds, causing interplanetary shocks, which are traveling shocks propagating out through the solar system. The magnetic field lines in the magnetic cloud were shown to have a helical geometry, as one expects for an approximately force-free (Beltrami) flux rope [11, 12]. Some laboratory experiments have also shown that the "Taylor relaxed state" generated through turbulence is well described as solutions of the force-free equation [13, 14]

In the next section, we will show that a more adequate formulation of the plasma dynamics allows a much wider class of special equilibrium solutions. The set of new solutions contains field configurations that can be qualitatively different from the force-free magnetic fields.

2.2 Coupled vortex dynamics in two-fluid MHD systems

The two-fluid model for the macroscopic dynamics of a plasma takes into account the difference between the electron and the ion velocities. Denoting the electron and ion flow velocity by $\boldsymbol{V}_e$ and $\boldsymbol{V}_i$, the macroscopic evolution equations become

$$\frac{\partial}{\partial t}\boldsymbol{V}_e + (\boldsymbol{V}_e \cdot \nabla)\boldsymbol{V}_e = \frac{-e}{m}(\boldsymbol{E} + \boldsymbol{V}_e \times \boldsymbol{B}) - \frac{1}{mn}\nabla p_e, \tag{2.15}$$

$$\frac{\partial}{\partial t}\boldsymbol{V}_i + (\boldsymbol{V}_i \cdot \nabla)\boldsymbol{V}_i = \frac{e}{M}(\boldsymbol{E} + \boldsymbol{V}_i \times \boldsymbol{B}) - \frac{1}{Mn}\nabla p_i, \tag{2.16}$$

where $\boldsymbol{E}$ is the electric field, p_e and p_i are the electron and the ion pressures respectively, e is the elementary charge, n is the number density of both electrons and ions (we consider a quasineutral plasma with singly charged ions), m and M are the electron and the ion masses, respectively. In the electron equation, the inertial terms [left-hand side of (2.15)] can be safely neglected, because of their small mass ($m \ll M$). Therefore, (2.15) reduces to

$$\boldsymbol{E} + \boldsymbol{V}_e \times \boldsymbol{B} + \frac{1}{en}\nabla p_e = 0. \tag{2.17}$$

When electron mass is neglected, the ion flow velocity can be expressed by the fluid velocity, $\boldsymbol{V}_i = \boldsymbol{V}$.

We write $\boldsymbol{V}_e = \boldsymbol{V} - \boldsymbol{j}/(en) = \boldsymbol{V} - \nabla \times \boldsymbol{B}/(\mu_0 en)$ and $\boldsymbol{E} = -\partial \boldsymbol{A}/\partial t - \nabla\phi$, where $\boldsymbol{A}$ and ϕ are the vector and scalar potential, respectively. Furthermore, choosing an arbitrary L_0 and B_0, we introduce the following set of dimensionless variables,

$$\begin{cases} \boldsymbol{x} = L_0\hat{\boldsymbol{x}}, \quad \boldsymbol{B} = B_0\hat{\boldsymbol{B}} \\ t = (L_0/V_A)\hat{t}, \quad p = (B_0^2/\mu_0)\hat{p}, \quad \boldsymbol{V} = V_A\hat{\boldsymbol{V}}, \\ \boldsymbol{A} = (L_0B_0)\hat{\boldsymbol{A}}, \quad \phi = (V_AL_0B_0)\hat{\phi}, \end{cases} \tag{2.18}$$

where the Alfvén velocity is given by $V_A = B_0/\sqrt{\mu_0 M n}$ (we assume $n =$ constant, for simplicity). Then (2.17) and (2.16) transform to the dimensionless set of equations,

$$\frac{\partial}{\partial\hat{t}}\hat{\boldsymbol{A}} = \left(\hat{\boldsymbol{V}} - \varepsilon\hat{\nabla}\times\hat{\boldsymbol{B}}\right)\times\hat{\boldsymbol{B}} - \hat{\nabla}\left(\hat{\phi} - \varepsilon\hat{p}_e\right), \tag{2.19}$$

$$\frac{\partial}{\partial\hat{t}}(\varepsilon\hat{\boldsymbol{V}} + \hat{\boldsymbol{A}}) = \hat{\boldsymbol{V}}\times\left(\hat{\boldsymbol{B}} + \varepsilon\hat{\nabla}\times\hat{\boldsymbol{V}}\right) - \hat{\nabla}\left(\varepsilon V^2/2 + \varepsilon\hat{p}_i + \hat{\phi}\right). \tag{2.20}$$

where the scaling coefficient $\varepsilon = l_i/L_0$ is a measure of the ion skin depth,

$$l_i = \frac{c}{\omega_{pi}} = \frac{V_A}{\omega_{ci}} = \sqrt{\frac{M}{\mu_0 ne^2}}.$$

The Hall term $\varepsilon(\hat{\nabla}\times\hat{\boldsymbol{B}})\times\hat{\boldsymbol{B}}$ of (2.19) and the fluid vorticity term $\varepsilon(\hat{\nabla}\times\hat{\boldsymbol{V}})\times\hat{\boldsymbol{V}}$ of (2.20), which may be regarded as a singular perturbation to the conventional

MHD equations, play an essential role in connecting the two different length scales, i.e., the characteristic length scale l_i, and a possible longer scale that describes the global structure of the system [36].

In what follows, we will take $L_0 = l_i$ (and hence, $\varepsilon = 1$), and simplify the notation by dropping the hat $\hat{}$ on the normalized variables. Taking the curl ($\nabla\times$) of (2.19) and (2.20), we can cast them in a revealing symmetric vortex equation

$$\frac{\partial}{\partial t}\boldsymbol{\omega}_j - \nabla \times (\boldsymbol{U}_j \times \boldsymbol{\omega}_j) = 0 \quad (j = 1, 2), \tag{2.21}$$

in terms of a pair of generalized vorticities

$$\boldsymbol{\omega}_1 = \boldsymbol{B}, \quad \boldsymbol{\omega}_2 = \boldsymbol{B} + \nabla \times \boldsymbol{V},$$

and the effective flows

$$\boldsymbol{U}_1 = \boldsymbol{V} - \nabla \times \boldsymbol{B}, \quad \boldsymbol{U}_2 = \boldsymbol{V}.$$

The vortex equation (2.21) indicates a coupling between the magnetic field and the plasma flow. The simplest and perhaps the most fundamental equilibrium solution to (2.21) is given by the "Beltrami condition" (2.3) , which implies the alignment of the vorticities and the corresponding flows. Assuming that a and b are constants, the Beltrami condition reads as a system of simultaneous

linear equations in $\boldsymbol{B}$ and $\boldsymbol{V}$

$$\boldsymbol{B} = a(\boldsymbol{V} - \nabla \times \boldsymbol{B}), \tag{2.22}$$

$$\boldsymbol{B} + \nabla \times \boldsymbol{V} = b\boldsymbol{V}. \tag{2.23}$$

These equations have a simple and significant connotation; the electron flow $(\boldsymbol{V} - \nabla \times \boldsymbol{B})$ parallels the magnetic field $\boldsymbol{B}$, while the ion flow $\boldsymbol{V}$ follows the "generalized magnetic field" $(\boldsymbol{B} + \nabla \times \boldsymbol{V})$. This generalized magnetic field contains the fluid vorticity induced by the ion inertia effect on a circulating flow.

2.3 Analytical structure

Combining (2.22) and (2.23) yields a second order partial differential equation

$$\nabla \times (\nabla \times \boldsymbol{u}) - (b - \tilde{a})\, \nabla \times \boldsymbol{u} + (1 - \tilde{a}b)\, \boldsymbol{u} = 0, \tag{2.24}$$

where $\tilde{a} = 1/a$ and $\boldsymbol{u} = \boldsymbol{B}$ or $\boldsymbol{V}$. It is convenient to denote the curl derivative $\nabla\times$ by "curl" to use it as an operator. Let us rewrite (2.24) in the form

$$(\mathrm{curl} - \lambda_+)(\mathrm{curl} - \lambda_-)\boldsymbol{u} = 0, \tag{2.25}$$

where

$$\lambda_\pm = \frac{1}{2}\left[(b - \tilde{a}) \pm \sqrt{(b + \tilde{a})^2 - 4}\right]. \tag{2.26}$$

Since the operators $(\mathrm{curl} - \lambda_\pm)$ commute, the general solution to the "double Beltrami equation" (2.25) is given by the linear combination of the two Beltrami fields. Let $\boldsymbol{G}_\pm$ be the Beltrami field such that

$$\begin{cases} (\mathrm{curl} - \lambda_\pm)\boldsymbol{G}_\pm = 0 & (\text{in } \Omega), \\ \\ \boldsymbol{n} \cdot \boldsymbol{G}_\pm = 0 & (\text{on } \partial\Omega), \end{cases}$$

where Ω ($\subset \boldsymbol{R}^3$) is a bounded domain with a smooth boundary $\partial\Omega$ and $\boldsymbol{n}$ is the unit normal vector onto $\partial\Omega$. Then, for arbitrary constants $C_\pm$, the double Beltrami magnetic field

$$\boldsymbol{B} = C_+\boldsymbol{G}_+ + C_-\boldsymbol{G}_-, \tag{2.27}$$

solves (2.25). The corresponding flow is given by

$$\boldsymbol{V} = (\lambda_+ + \tilde{a})\, C_+\boldsymbol{G}_+ + (\lambda_- + \tilde{a})\, C_-\boldsymbol{G}_-. \tag{2.28}$$

Therefore, the existence of a nontrivial solution to the double curl Beltrami equations (2.24) will be predicated on the existence of the appropriate pair of single Beltrami fields. Let us briefly review the mathematical theory of single Beltrami fields.

Suppose that Ω ($\subset \boldsymbol{R}^3$) is a bounded domain with a smooth boundary. We

consider

$$\begin{cases} \nabla \times \boldsymbol{u} = \lambda \boldsymbol{u} & (\text{in } \Omega), \\ \\ \boldsymbol{n} \cdot \boldsymbol{u} = 0 & (\text{on } \partial\Omega), \end{cases} \tag{2.29}$$

where λ is a complex constant number. The spectral theory of the curl operator reveals an interesting relation of this problem with the cohomology theory. We have the following theorem [3].

(i) If Ω is simply connected, then (2.29) has a non-zero solution for special λ included in a set of discrete real numbers; these numbers represent the point spectrum of the self-adjoint part of the curl operator.

(ii) If Ω is multiply connected, then (2.29) has a non-zero solution for every $\lambda \in \mathbf{C}$.

In a multiply connected domain, the solution of the double curl Beltrami equation is given by a linear combination of two single Beltrami fields that exist for arbitrary Beltrami parameters.

It is important to note that the double Beltrami field (2.27) encompasses a wide class of steady-state equations of mathematical physics. The conventional force-free field equation $\nabla \times \boldsymbol{B} - \lambda \boldsymbol{B} = 0$, which describes paramagnetic fields,

is included in this system as a special case: $\lambda_\pm$ are real and one of $C_\pm$ is zero or $\lambda_+ = \lambda_-$. On the other hand, when $\lambda_\pm$ are pure imaginary and one of $C_\pm$ is zero or $\lambda_+ = \lambda_-$, (2.27) resembles well-known fully diamagnetic solutions to the London's equation of super conductivity. We note that, in this version of the London equation, the characteristic shielding length for the magnetic field is the ion skin depth c/ω_{pi}, instead of the usual electron skin depth c/ω_{pe}, because it is the ion-dynamics that brings about the coupling of the magnetic field with the collective motion of the medium.

2.4 Conservation laws

The conservation of helicity applies for general vortex dynamics. Let $\boldsymbol{\omega}$ be a vorticity that satisfies (2.1) and boundary condition

$$\boldsymbol{n} \times (\boldsymbol{U} \times \boldsymbol{\omega}) = 0 \quad (\text{on } \partial\Omega). \tag{2.30}$$

The general "helicity" is defined as

$$h = \frac{1}{2} \int_\Omega (\mathrm{curl}^{-1}\boldsymbol{\omega}) \cdot \boldsymbol{\omega} \, \mathrm{d}^3x, \tag{2.31}$$

where curl^{-1} is the inverse operator of the curl that is represented by the Biot-Savart integral. By this definition, we easily verify the conservation of h.

For our two-fluid MHD model (2.21), we have two helicities

$$h_1 = \frac{1}{2}\int_\Omega \boldsymbol{A}\cdot\boldsymbol{B}\ \mathrm{d}^3x, \tag{2.32}$$

$$h_2 = \frac{1}{2}\int_\Omega (\boldsymbol{A}+\boldsymbol{V})\cdot(\boldsymbol{B}+\nabla\times\boldsymbol{V})\ \mathrm{d}^3x. \tag{2.33}$$

The total energy

$$E = \frac{1}{2}\int_\Omega \left(\boldsymbol{B}^2+\boldsymbol{V}^2\right)\ \mathrm{d}^3x, \tag{2.34}$$

is also conserved [37].

2.5 Generalized Bernoulli condition

As we have shown in (2.4), the Beltrami condition directly leads the generalized Bernoulli condition, which expresses the homogeneous energy density. In two-fluid MHD systems, going back from (2.21) to the original (decurled) equations (2.19) and (2.20), we find φ_j, which corresponds to the energy density of each fluid, as

$$\varphi_1 = \phi - p_e, \tag{2.35}$$

$$\varphi_2 = V^2/2 + \phi + p_i. \tag{2.36}$$

Subtracting (2.35) from (2.36) under the Bernoulli condition $\varphi_j = \text{const}$, we obtain

$$\beta + V^2 = \text{const}, \tag{2.37}$$

where β is a conventional beta ratio that is given by $\beta = 2(p_e + p_i)$ in the normalized unit. This relation shows that the double Beltrami equilibrium is no longer zero-beta (force-free), but it can confine an appreciable pressure when an appreciable flow (in the Alfvén unit) is driven.

At the end of this chapter, in order to make it clear how the double Beltrami field is classified as a relaxed state, we summarize the hierarchy of the relaxed state in Fig. 2.1. In applying a magnetic field, current, and flow to the plasma, the energy of the system rises up with adding harmonic (zero Beltrami) field, single and the double Beltrami fields. These "energy levels" are explained as follows. The absolute minimum energy state is the vacuum. Suppose that we apply a static magnetic field (harmonic field) and produce a plasma. Without applying any drive, the plasma will disappear and the system will relax into the harmonic magnetic field. If we drive the plasma current to sustain the magnetic helicity h_1, the plasma relaxes into the Taylor state and achieves the Beltrami magnetic field [5]. When a strong flow exists in addition to the current in a two-component plasma, the system must conserve two distinct helicities h_1 and

h_2 and the self-organized state becomes qualitatively different from the Taylor relaxed state. The two-fluid effect induces a coupling among the flow, magnetic field, electric field and the pressure, resulting in a "singular perturbation" to the MHD system. To access these states one must also maintain the second helicity invariant h_2 by driving and sustaining an appropriate flow. As the final state becomes more and more complex, greater and greater care is needed for its creation and maintenance. However, all requirements are met, the field structures may relax into the double Beltrami field [15, 16].

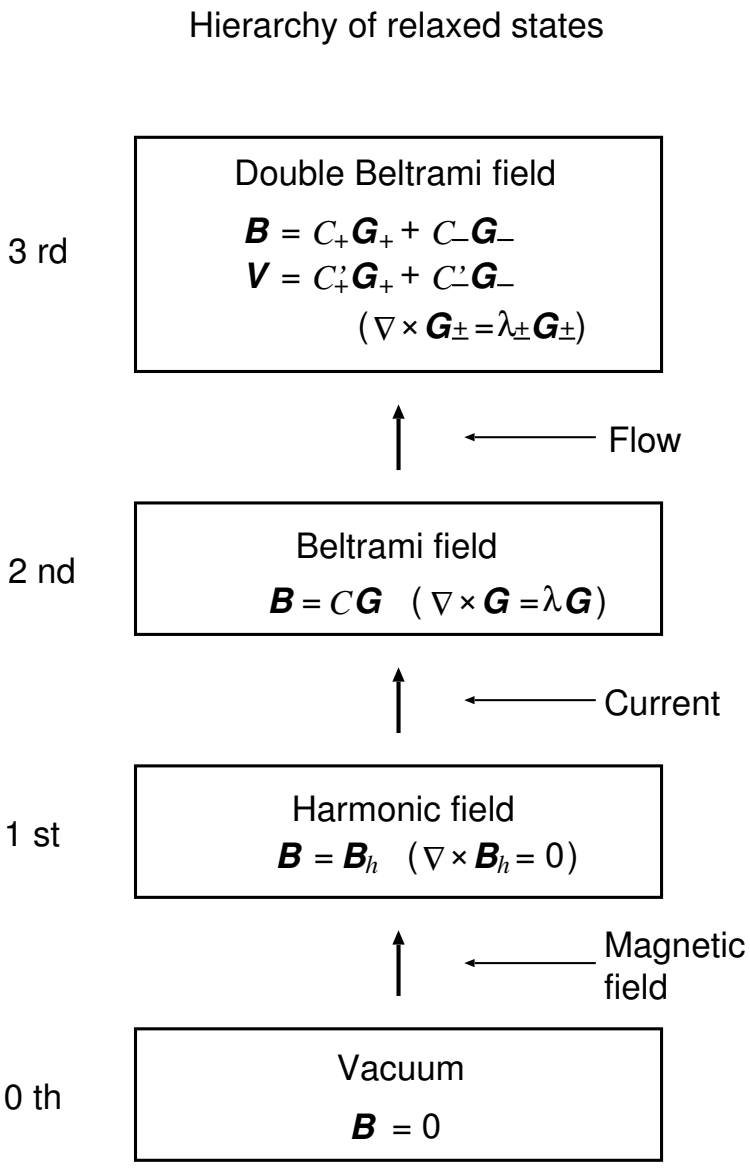

Figure 2.1: Hierarchy of relaxed states.

Chapter 3

Algebraic structure in relaxed plasmas and application to the solar corona

3.1 Introduction

Eruptive processes in the solar atmosphere, such as flares, erupting prominences, or coronal mass ejections (CMEs), are associated with the transition from a slow evolution, during which apparently excess energy is built up to a fast dynamic evolution that involves a rapid energy transfer to plasma kinetic

energy in the form of heat and bulk motion, most likely from excess magnetic energy. Flares, erupting prominences, and CMEs may happen separately but can also be parts of a more global dynamic process.

These solar eruptive events, which are believed to result mainly from a sudden release of magnetic energy stored in the corona, are primarily MHD processes. There are many models that try to explain these processes, using MHD theory. In most of them, it is assumed that the coronal magnetic field is based on the Beltrami field, $\nabla \times \boldsymbol{B} = \lambda \boldsymbol{B}$, which represents a Taylor (force-free) relaxed state of an ideal MHD [38] - [41]. Since the magnetic field strength is markedly high and the beta ratio is low in the solar corona, the Beltrami magnetic field is considered the most reliable configuration, at least on a large scale.

The solar eruptive events are associated with the termination of an equilibrium sequence (the catastrophic behavior of an equilibrium), or an instability [42]. It may be conceptually more convincing to associate an eruptive event with a catastrophe in the equilibrium evolution rather than the onset of a linear instability. The catastrophe is defined by a critical behavior in the equilibrium evolution characterized by a monotonically changing control parameter, which in many cases corresponds only to an equilibrium bifurcation.

For the solar flare, this concept has been followed by numerous investigators ([40] - [45] and the references therein).

TRACE (Transition Region and Coronal Explorer) provides an unprecedented view of the solar outer atmosphere. It observed that a corona is extremely dynamic and full of flows [17]-[20]. In this chapter, in order to take the flow effect into account, we use a collisionless two-fluid model. As mentioned in Chap. 2, this model leads to a more general relaxed state called a double Beltrami field. In a two-fluid model, the magnetic field and the velocity field are self-consistently related by the singular perturbation, and these fields can be expressed by the superposition of two different Beltrami fields. These fields cover a vast region of steady states far richer than the conventional Beltrami (force-free) field and, hence, the equilibria achieved help us to understand a variety of structures generated in the solar corona (see, e.g. [46], where it is shown that broad variety of coronal structures, including coronal holes as well as different kind eruptions, are created from the interaction of plasma flows with the magnetic fields anchored in the sun).

After giving a brief summary of phenomenology and observations of the sun (Sec. 3.2), the double Beltrami field is applied to the quiescent sun closed coronal structures because of its simple mathematical expression in order to

treat an equilibrium bifurcation analytically, and one set of algebraic equations is derived (Sec. 3.3). Analyzing these equations, we show that, if the total energy is larger than a certain critical energy, when flux loops become close to each other, the loops interact strongly and suddenly loose their equilibria. Further it is sown that, when it happens, a magnetic field is reduced to a single Beltrami field and its energy is minimized (Sec. 3.4). We consider an example of the double Beltrami fields in a solar coronal scale. In this case, we indicate that almost all the magnetic energy is transfered to the flow energy and a solar eruption occurs (Sec. 3.5).

3.2 Phenomenology and observations of the sun

3.2.1 Plasma flows in the corona

There are several recent publications [17]-[28] cataloging enough observational evidence for flows in the regions between the sun and the corona. A comprehensive description and evaluation of the published data is beyond the scope of our theory. But a relatively short and suggestive survey is certainly indicated.

To begin with there is the evidence from UVCS on SOHO. A measurement of the intensity ratio of the OVI ion emission doublet ($\lambda 1037A$ and $\lambda 1032A$) seems to point to plasma outflows in the inner and middle corona with velocities (90-400) km/s [21]. SOHO observations, though, need a very careful interpretation.

Studying the extreme ultraviolet (EUV) and soft X-ray (SXR) loops, the authors of [22] suggested "That macroscopic coronal loop would be filled by the up-flowing plasma in cycles of 5-10 minutes." The loop life-times were found of the order of 10-40 minutes with flow velocities $\sim$ (50-100) km/s. It was outlined the static loop models can not explain their observations, but loop models with spatial fine structure (e.g. strands) and temporal variability (e.g. episodic heating cycles) seem to required. The origin of the flows that could fill the loops or create the hot coronal loops, is still unknown. Though a few mechanisms like the reconnection processes in chromospheric network are already in vogue, much work needs to be done for a desirable understanding of their existence and nature. The possible up-flows could be those from the chromosphere (dubbed chromospheric evaporation). One must, however, remember that estimates given in [19] point out that "the energy content in EUV, SXR and hard X-ray (HXR) nano- and microflares in insufficient (by 2-3 orders of magnitude) to

account for coronal heating."

There is another class of small-scale features that could play a role in the creation of coronal structures - these are the short-lived (minutes) jets observed at the base of the corona [23]-[25]. "When observed with high spatial resolution, the atmosphere at the base of the corona is found to be dynamic with a large fraction of the surface covered by chromospheric and transition region material moving up and down in structures with characteristic sizes of $\sim$ 1000 km."

We end this short survey by a quote from [18] on the TRACE observations; "The EUV observations by TRACE reveal not only material at coronal temperatures moving upward from as low as a few thousand kilometers above the photosphere, but also cool material, no hotter than about 20,000 K. Perhaps we are seeing material being thrust upward by strong Lorentz forces associated with rapid field deformation, as well as by sudden heat deposition by current dissipation. Understanding the details of these processes leading to these injections of matter into the outer atmosphere may well be key to solving the riddle of coronal heating."

The evidence for the flows is by no means overwhelming but it is enough to make them an important element of the solar corona - they provide a tremen-

dous diversity for coronal structures as well as the basic energy for primary heating. For this research, therefore, we shall simply exploit that the flows exist, and work out consequences with their effect.

3.2.2 Solar flares and catastrophe theory

Solar flares are among the most energetic and enigmatic phenomena in the solar atmosphere. Large amount of energy (10^{29} - 10^{32} erg) are suddenly released in the corona to produce heating, mass motion, acceleration of charged particles, shocks, and emission of electromagnetic radiation. It is believed that a flare may be a transient phenomenon showing a rapid increase (followed by either rapid or gradual decay) in some electromagnetic waves. In this definition, the absolute value of the peak intensity itself does not matter. Hence we call micro-flares for transient phenomena with energy of order of 10^{25} - 10^{27} erg, and nano-flares for those with energy of 10^{22} - 10^{24} erg [47]. Historically, flares were found as sudden brightenings in Hα monochromatic images and (rarely) in white light images. Later flares have been observed by radio waves and X-rays. From detailed imaging observations of flares, we find that most flares occur in active regions, i.e., in the region of strong magnetic field near sunspots.

In Hα, large flares often show bright two ribbons; such flares are called

two-ribbon flares. The two ribbons have length of 10^5 km and width of some 10^4 km, and are parallel to the polarity-inversion line, which suggests that they are footpoints of arcades overlying the inversion line. Large two ribbon flares are often associated with filament eruptions and/or coronal mass ejections (CMEs). On the other hand, there are many flares that are not associated with CMEs; such flares are relatively compact, and have magnetic field configurations that do not seem to change much.

It was once considered that CMEs are kind of blast waves or shocks produced by sudden pressure enhancements in flares. It has become clear, however, that some of large flares are preceded by the start of CME. That is, flares are not the origin of CMEs, but both flares and CMEs seem to have the same origin, which may be a kind of MHD instability or loss of equilibrium occurring in the global magnetic configuration of the corona. There are various suggestive publications that consider different flare models [48]. We will present our view of this problem below.

An interesting possibility is proposed that mass ejections are driven by changes in the very large scale magnetic fields that occur within coronal structures, such as helmet streamers, and have only a coincidental relationship to smaller scale magnetic fields that seem to be involved in solar flares [49].

It is conceptually more convincing to associate an eruptive event with a loss of equilibrium, Fig. 3.1 (a), or a jump in the equilibrium evolution, Fig. 3.1 (b), rather than the onset of a linear instability. These catastrophic behaviors correspond only to equilibrium bifurcations. Catastrophe may be defined that "critical (discontinuous) behavior in the equilibrium evolution follows continuous change of a control parameter". For explaining the solar flares, there are many models which use this concept ([40] - [45] and the references therein).

As mentioned before, TRACE observed that the corona is very dynamical. Further, we can find the following facts; Yohkoh data provided SXT images where quite unambiguous examples of magnetic loops that collide and interact with the release of energy [9].

Thus, for the sake of expressing dynamical interacting loops, we will chose a length scale of the the coronal loop structure as a control parameter.

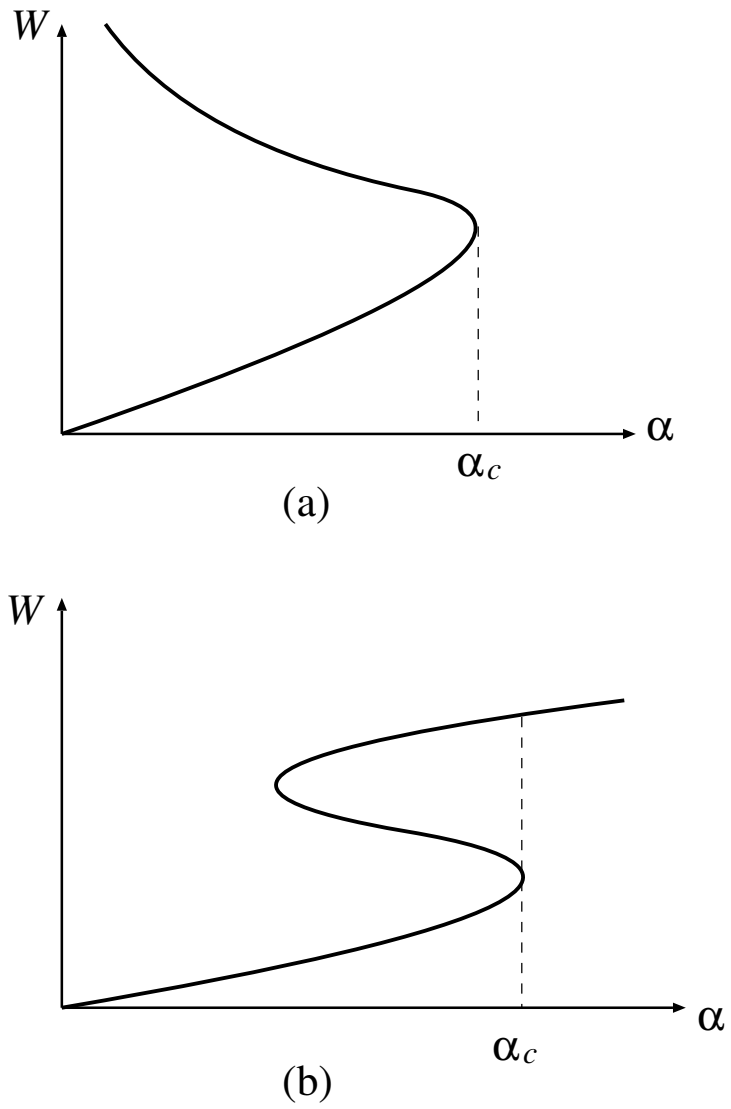

Figure 3.1: α and W are respectively some relevant control parameter and equilibrium quantity. (a) loss of equilibrium for $\alpha > \alpha_c$, (b) jump of W at $\alpha = \alpha_c$.

3.3 Conservation laws and algebraic structure

To study the solar eruptive events, we model the coronal quasi-equilibrium magnetic field using the double Beltrami field. Advantages of this modeling are summarized as follows;

(i) We can take the flow effect into account self-consistently.

(ii) Separating two scales, for instance $\lambda_+ << \lambda_-$, we can treat the coronal magnetic field as a single Beltrami field in a macro scale, which is the scale of $1/\lambda_+$.

(iii) Structures show far richer behavior than just a single Beltrami field because of the existence of micro scale component $(1/\lambda_-)$.

We just want to note here that, as we mentioned above, observations reveal that the time required to create the hot coronal structure is of the order of few minutes and is shorter than the life-time of this bright formation. As it was shown in [46], we have to distinguish two important eras in the life of a coronal structure: a hectic period when it acquires particles and energy, and the relatively calmer period when it shines as a bright, high temperature ob-

ject. The cases of eruptive events according to observations can be divided in two different classes: (a) case when already hot structure (primarily heated) at some moment undergoes the catastrophe and gets magnetic field energy excess in a very short time, and (b) when creating hot structure without passing through the long-living time-period (due to structure-structure-flow interactions or other processes) distorts and releases energy. In both cases, it is necessary that, at some stage of evolution, flow energy is somewhat greater than magnetic energy - hence, either we have a sharp increase of temperature of a structure or we have a strong and sharp deformation (distortion) of the structure. In our analysis, we keep the temperature varying, but as it was assumed above, density was considered constant for the given structure. This is a rather drastic step but it can help us a great deal in unraveling the underlying physics. There are two entirely different situations where this assumption may be justified:

(i) The primary heating of corona has already been performed, i.e., a substantial part of flow initial kinetic energy has been converted to heat. The rest of the kinetic energy, i.e., the kinetic energy of the equilibrium coronal structure is not expect to change much within the span of a given structure. There will be exceptional cases like the neighborhood

of the coronal holes and streamer belt, where significant heating could still be going on, and the temperature and density variations could not be ignored. Such regions are extremely hard to model.

(ii) If the rates of kinetic energy dissipation are not very large, we can imagine the plasma to be going through a series of quasi-equilibria before it settles into a particular coronal structure. At each stage we need the velocity fields in order to know if an appropriate amount of heating can take place. The density variation, though a factor, is not crucial in an approximate estimation of the desired quantities.

Now, after these discussions, in order to consider an equilibrium bifurcation, first, we have to treat it algebraically. Therefore, in this section, we derive a set of algebraic relations that express equilibria. As shown in Sec. 2.3, the double Beltrami field is characterized by four parameters (two eigenvalues and two amplitudes);

$$\begin{cases} \lambda_+,\ \lambda_-, \\ C_+,\ C_-. \end{cases} \tag{3.1}$$

To determine these parameters, we can invoke the constants of motion of the evolution equation, that is, h_1, h_2, and E, expressed by (2.32) - (2.34). Using these three constants of motion, and choosing the λ_+ as a "control parameter",

which characterizes the larger length scale of the structure (assuming $|\lambda_+| < |\lambda_-|$), we can cast the analysis of double Beltrami fields into algebraic relations. Note, that it is convenient to make such a choice since as the observations as well different publications (see e.g. [50] - [52] and the references therein) indicate in the process of structure-structure interactions the deformation or even distortion of their "initial" shapes take place. We show that depending on the initial and boundary conditions the rate of this deformation is different.

Here, as $\boldsymbol{G}_\pm$ in (2.27) and (2.28), we consider one of the simplest Beltrami eigenfunctions, 2-D (two-dimensional) ABC vector field,

$$\boldsymbol{G}_\pm = g_{x\pm} \begin{pmatrix} 0 \\ \sin \lambda_\pm x \\ \cos \lambda_\pm x \end{pmatrix} + g_{y\pm} \begin{pmatrix} \cos \lambda_\pm y \\ 0 \\ \sin \lambda_\pm y \end{pmatrix}, \tag{3.2}$$

in a cubic volume that has sides of length L. To study the problem of coronal structure-structure interaction as long as the energy transfer conditions, we assume the periodic boundary conditions and let the constants $g_{x\pm}$ and $g_{y\pm}$ satisfy

$$(g_{x\pm})^2 + (g_{y\pm})^2 = 1, \tag{3.3}$$

where the ratio of $g_{x\pm}$ and $g_{y\pm}$ defines the shape of an arcade. In Fig. 3.2 we show the field line structure of a 2-D ABC vector field that resembles a coronal

loop. If $\lambda_{\pm}$ are complex in (3.2), the equilibrium solution will have the spatially decaying (or growing) component initially. Such regions are extremely hard to model and it is beyond the scope of present analysis. In this study, we choose real $\lambda_{\pm}$ for coronal quasi-equilibrium structures.

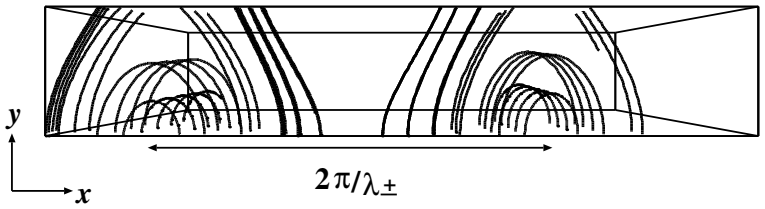

Figure 3.2: Magnetic field line structure of a two-dimensional ABC map resembling a coronal arcade.

Assuming

$$L = n_+ \frac{2\pi}{\lambda_+} = n_- \frac{2\pi}{\lambda_-}, \qquad (3.4)$$

$$(n_{\pm}; \text{integer})$$

$\boldsymbol{G}_{\pm}$ of (3.2) satisfy the following relations,

$$\int_{\Omega} \boldsymbol{G}_{\pm}^2 \, \mathrm{d}^3x = L^2 \left[(g_{x\pm})^2 + (g_{y\pm})^2 \right] = L^2, \qquad (3.5)$$

$$\int_\Omega \boldsymbol{G}_+ \cdot \boldsymbol{G}_- \, \mathrm{d}^3x = 0, \tag{3.6}$$

where $\int_\Omega \mathrm{d}^3x = \int_0^L \int_0^L \mathrm{d}x\mathrm{d}y$. Therefore, expressing

$$\begin{aligned} \boldsymbol{A} &= \frac{C_+}{\lambda_+}\boldsymbol{G}_+ + \frac{C_-}{\lambda_-}\boldsymbol{G}_-, & (3.7)\\ \nabla \times \boldsymbol{V} &= \lambda_+ (\lambda_+ + \tilde{a}) C_+ \boldsymbol{G}_+ + \lambda_- (\lambda_- + \tilde{a}) C_- \boldsymbol{G}_-, & (3.8) \end{aligned}$$

the constants of motion h_1, $\tilde{h}_2 (= h_2 - h_1)$ and E read

$$\begin{aligned} h_1 &= \frac{L^2}{2}\left[\frac{C_+^2}{\lambda_+} + \frac{C_-^2}{\lambda_-}\right], & (3.9)\\ \tilde{h}_2 &= \frac{L^2}{2}\Big\{[2 + \lambda_+ (\lambda_+ + \tilde{a})] (\lambda_+ + \tilde{a}) C_+^2 \\ &\qquad + [2 + \lambda_- (\lambda_- + \tilde{a})] (\lambda_- + \tilde{a}) C_-^2 \Big\}, & (3.10)\\ E &= \frac{L^2}{2}\Big\{\left[1 + (\lambda_+ + \tilde{a})^2\right] C_+^2 \\ &\qquad + \left[1 + (\lambda_- + \tilde{a})^2\right] C_-^2 \Big\}. & (3.11) \end{aligned}$$

Next we will derive a general relation of equilibrium. We rewrite (3.9) - (3.11) in a more revealing form in order to represent characteristics of an equilibrium. Here we summarize basic relations for convenience of following calculations,

$$(\lambda_+ + \tilde{a})^{-1} = (\lambda_- + \tilde{a}), \tag{3.12}$$

$$\lambda_+ + \lambda_- = b - \tilde{a}, \tag{3.13}$$

$$\lambda_+\lambda_- = 1 - b\tilde{a}, \tag{3.14}$$

$$\tilde{a} = \frac{1}{2}\left[-\left(\lambda_+ + \lambda_-\right) \pm \sqrt{\left(\lambda_+ - \lambda_-\right)^2 + 4}\right], \tag{3.15}$$

$$b = \frac{1}{2}\left[\left(\lambda_+ + \lambda_-\right) \pm \sqrt{\left(\lambda_+ - \lambda_-\right)^2 + 4}\right]. \tag{3.16}$$

Using these relations, it turns out that $\tilde{h}_2$ of (3.10) can be easily expressed in terms of h_1, E, λ_+, λ_- (or h_1, E, $\tilde{a}$, b). We notice that

$$\begin{aligned}
\tilde{h}_2 &= \frac{L^2}{2}\left\{\left[2\left(\lambda_- + \tilde{a}\right) + \lambda_+\right]\left(\lambda_+ + \tilde{a}\right)^2 C_+^2\right. \\
&\qquad \left. + \left[2\left(\lambda_+ + \tilde{a}\right) + \lambda_-\right]\left(\lambda_- + \tilde{a}\right)^2 C_-^2\right\} \\
&= \frac{L^2}{2}\left[\left(\lambda_- + b + \tilde{a}\right)\left(\lambda_+ + \tilde{a}\right)^2 C_+^2\right. \\
&\qquad \left. + \left(\lambda_+ + b + \tilde{a}\right)\left(\lambda_- + \tilde{a}\right)^2 C_-^2\right] \\
&= \frac{L^2}{2}\left\{\left[b\left(\lambda_+ + \tilde{a}\right)^2 + \left(\lambda_+ + \tilde{a}\right)\right] C_+^2\right. \\
&\qquad \left. + \left[b\left(\lambda_- + \tilde{a}\right)^2 + \left(\lambda_- + \tilde{a}\right)\right] C_-^2\right\} \\
&= \frac{L^2}{2}\left\{\left[b\left(\lambda_+ + \tilde{a}\right)^2 + \left(b - \lambda_-\right)\right] C_+^2\right. \\
&\qquad \left. + \left[b\left(\lambda_- + \tilde{a}\right)^2 + \left(b - \lambda_+\right)\right] C_-^2\right\} \\
&= b\frac{L^2}{2}\left\{\left[1 + \left(\lambda_+ + \tilde{a}\right)^2\right] C_+^2 + \left[1 + \left(\lambda_- + \tilde{a}\right)^2\right] C_-^2\right\} \\
&\qquad -\lambda_+\lambda_-\frac{L^2}{2}\left[\frac{C_+^2}{\lambda_+} + \frac{C_-^2}{\lambda_-}\right] \\
&= bE - \lambda_+\lambda_- h_1,
\end{aligned} \tag{3.17}$$

which can be cast in several equivalent forms

$$h_2 = h_1 + \tilde{h}_2 = b\,(E + h_1\tilde{a})\,, \tag{3.18}$$

$$\tilde{h}_2 = \frac{E}{2}\left[(\lambda_+ + \lambda_-) \pm \sqrt{(\lambda_+ - \lambda_-)^2 + 4}\right] - \lambda_+\lambda_- h_1. \tag{3.19}$$

For given h_1, E, $\tilde{h}_2$ (or h_2) and λ_+ (control parameter), we solve (3.19) to find λ_-. Here we assume that L is sufficiently large, so that $\lambda_\pm$ $(= n_\pm/L)$ can take continuous real values. From (3.18), we know that this equilibrium makes the free energy zero [36, 37];

$$E - \tilde{a}h_1 + \frac{1}{b}h_2 = 0. \tag{3.20}$$

From (3.9) and (3.11), C_+ and C_- are now given by

$$\frac{L^2}{2}C_+^2 = D^{-1}\left\{E - \left[1 + (\lambda_- + \tilde{a})^2\right]\lambda_- h_1\right\}\lambda_+, \tag{3.21}$$

$$\frac{L^2}{2}C_-^2 = D^{-1}\left\{E - \left[1 + (\lambda_+ + \tilde{a})^2\right]\lambda_+ h_1\right\}\lambda_-, \tag{3.22}$$

where

$$D = \left[1 + (\lambda_+ + \tilde{a})^2\right]\lambda_+ - \left[1 + (\lambda_- + \tilde{a})^2\right]\lambda_- = (\lambda_+ - \lambda_-)\,b\,(b + \tilde{a}) \tag{3.23}$$

3.4 Analysis of the equilibrium states

In this section, we will discuss the solutions expressed by (3.19), (3.21) and (3.22), that is, behavior of parameters λ_-, C_+ and C_- defined by the control parameter λ_+, which characterizes larger length scale. When $h_1 = 1$, $h_2 = 5$, $E = 2$ and $h_1 = 1$, $h_2 = 5$, $E = 4$, the physical quantities λ_- and $C_\pm$ that determine an equilibrium, are plotted as the functions of λ_+ in Fig. 3.3 and Fig. 3.4, respectively. Here we set $C_\pm > 0$ and $L^2/2 = 1$. It dose not contradict the assumption of large L because the nature of this system of equations is independent of L (see note [53]). Dashed lines of λ_- and C_+ in these figures correspond to the region of imaginary C_-. Comparing these figures we find that the behavior of solutions change drastically depending on E. In Fig. 3.3, λ_- and $C_\pm$ change continuously with varying λ_+. It means that, when the larger scale of the structure $(1/\lambda_+)$ changes continuously the equilibrium expressed by (3.2) still may exist with changing physical parameters (note that if λ_+ is too small then C_- becomes imaginary - this case we won't discuss here). Thus, even though the quantity changes the quality is kept. In Fig. 3.4, situation changes drastically when λ_+ becomes larger than some critical value $\lambda_+^{\rm crit}$ (when the larger length scale is small) - we see that an equilibrium is lost.

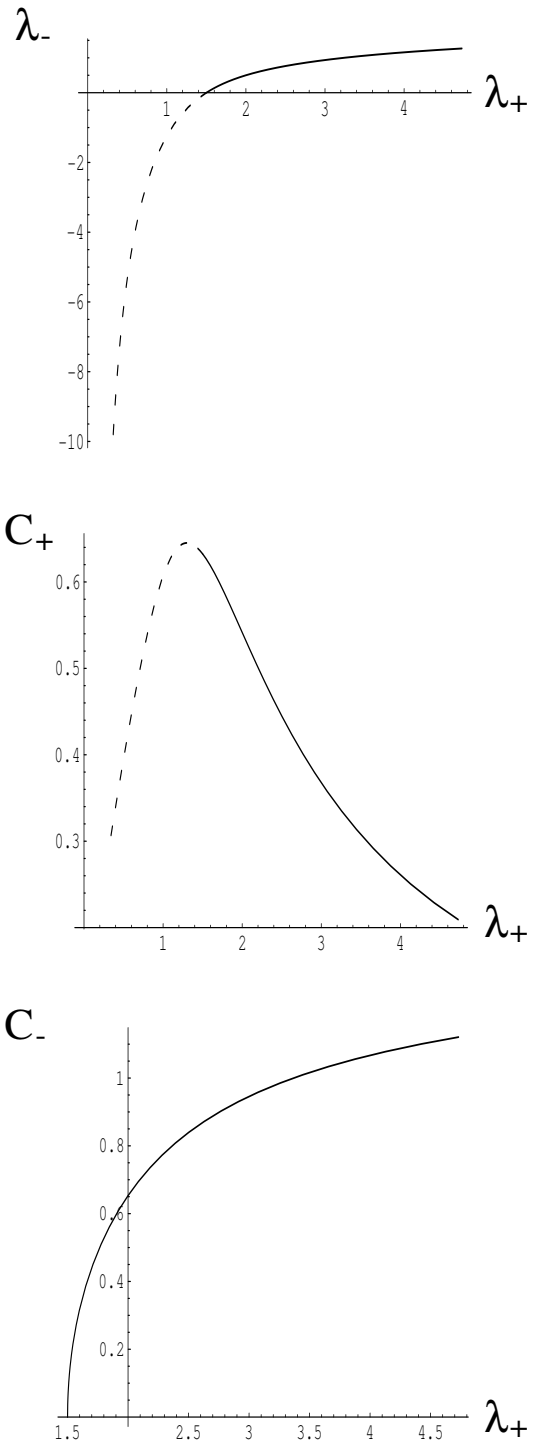

Figure 3.3: Solution of λ_- and $C_\pm$ for $h_1 = 1$, $h_2 = 5$ and $E = 2$.

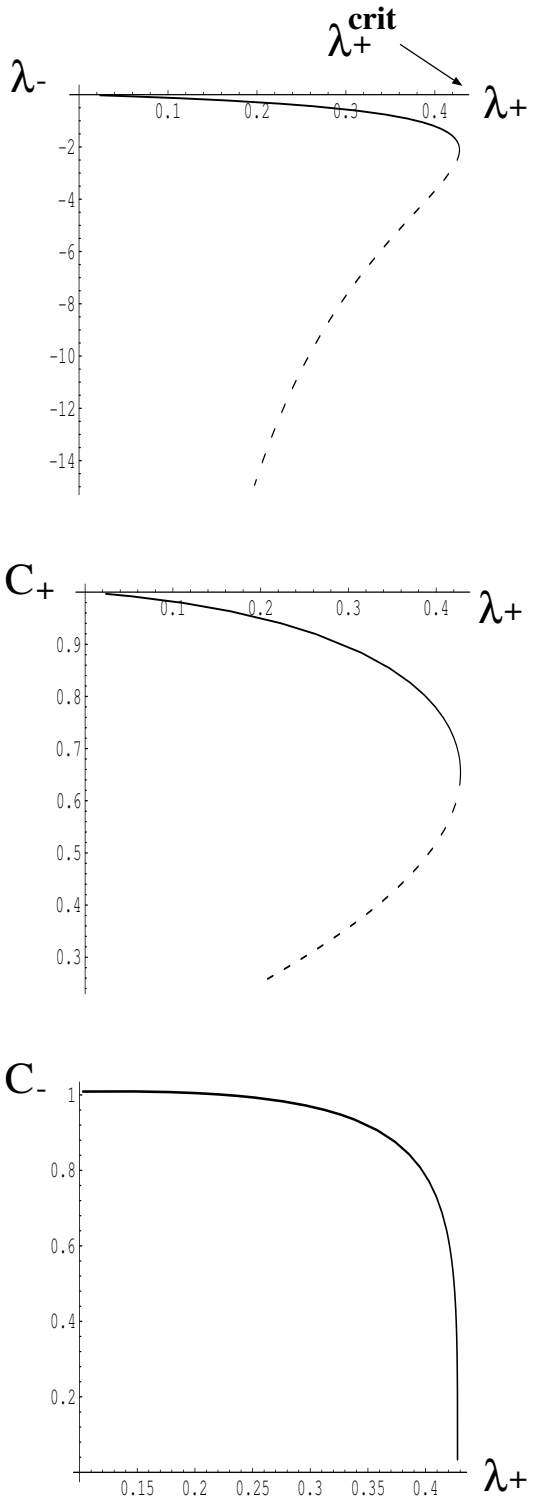

Figure 3.4: Solution of λ_- and $C_\pm$ for $h_1 = 1$, $h_2 = 5$ and $E = 4$. If the energy E is large, the equilibrium solution is lost when the length scale $1/\lambda_+$ is decreased.

From now on, we will study mainly the latter type of solution. First, we find a condition for the catastrophic behavior as shown in Fig. 3.4. Let's use the equivalent equation (3.18) instead of (3.19). The equation (3.18) is written as

$$b = \frac{h_2}{E + h_1 \tilde{a}}, \tag{3.24}$$

where we assume that $E + h_1\tilde{a} \neq 0$. Using (3.24), one can express $\lambda_\pm$ and $C_\pm$ by the parameter $\tilde{a}$. Then the condition of critical point $\mathrm{d}\lambda_+/\mathrm{d}\lambda_- = 0$ demands to have $\mathrm{d}\lambda_+/\mathrm{d}\tilde{a} = 0$. From (2.26) we find

$$\begin{aligned} \frac{\mathrm{d}\lambda_+}{\mathrm{d}\tilde{a}} &= \frac{1}{2}\left[\left(-1 + \frac{b+\tilde{a}}{\sqrt{(b+\tilde{a})^2 - 4}}\right)\right. \\ &\qquad \left. + \frac{\mathrm{d}b}{\mathrm{d}\tilde{a}}\left(1 + \frac{b+\tilde{a}}{\sqrt{(b+\tilde{a})^2 - 4}}\right)\right] \\ &= 0, \end{aligned} \tag{3.25}$$

which leads to

$$\begin{aligned} \frac{\mathrm{d}b}{\mathrm{d}\tilde{a}} &= \frac{-\left[-1 + (b+\tilde{a})/\sqrt{(b+\tilde{a})^2 - 4}\right]}{\left[1 + (b+\tilde{a})/\sqrt{(b+\tilde{a})^2 - 4}\right]} \\ &= -\frac{1}{4}\left[(b+\tilde{a}) - \sqrt{(b+\tilde{a})^2 - 4}\right]^2 \\ &= -(\lambda_- + \tilde{a})^2 . \end{aligned} \tag{3.26}$$

On the other hand, (3.24) gives

$$\frac{\mathrm{d}b}{\mathrm{d}\tilde{a}} = \frac{-h_1 h_2}{\left(E + h_1 \tilde{a}\right)^2}. \tag{3.27}$$

From the equations (3.26) and (3.27) we get

$$h_1 h_2 = \left[\left(\lambda_- + \tilde{a}\right)\left(E + h_1 \tilde{a}\right)\right]^2 \geq 0, \tag{3.28}$$

which implies that, when two helicities h_1 and h_2 have opposite signs, we can not observe the loss of equilibrium. The above equation reads as

$$\begin{aligned} \mp 2\sqrt{h_1 h_2} &= \left[\left(b + \tilde{a}\right) - \sqrt{\left(b + \tilde{a}\right)^2 - 4}\right]\left(E + h_1 \tilde{a}\right) \\ &= h_2 + \tilde{a}\left(E + h_1 \tilde{a}\right) \\ &\quad - \sqrt{\left[h_2 + \tilde{a}\left(E + h_1 \tilde{a}\right)\right]^2 - 4\left(E + h_1 \tilde{a}\right)^2}. \end{aligned} \tag{3.29}$$

Rearranging this equation with respect to $\tilde{a}$, we get

$$\begin{aligned} \left(h_1^2 \pm h_1\sqrt{h_1 h_2}\right)\tilde{a}^2 + \left(2h_1 \pm \sqrt{h_1 h_2}\right) E\tilde{a} & \\ + E^2 + h_1 h_2 \pm h_2\sqrt{h_1 h_2} &= 0. \end{aligned} \tag{3.30}$$

Then $\tilde{a}$ has a real solution to $\mathrm{d}\lambda_+/\mathrm{d}\tilde{a} = 0$, if

$$\begin{aligned} &\left[\left(2h_1 \pm \sqrt{h_1 h_2}\right) E\right]^2 \\ &\quad -4\left(h_1^2 \pm h_1\sqrt{h_1 h_2}\right)\left(E^2 + h_1 h_2 \pm h_2\sqrt{h_1 h_2}\right) \\ &= h_1 h_2 E^2 - 4h_1 h_2\left(h_1 \pm \sqrt{h_1 h_2}\right)^2 \\ &\geq 0. \end{aligned} \tag{3.31}$$

Hence, dividing (3.31) by $h_1 h_2 > 0$, we can conclude that a loss of equilibrium occurs when the following inequality holds;

$$E^2 \geq E_c^2 = 4\left(h_1 \pm \sqrt{h_1 h_2}\right)^2. \tag{3.32}$$

It may be significant to state that, if the condition (3.32) is satisfied, $\lambda_\pm$ can be complex. That is, (3.32) is equivalent to the condition that a line expressed by (3.24) passes the region where $(b+\tilde{a})^2 < 4$ on $\tilde{a}$-b plane; $(b+\tilde{a})^2 < 4$ leads to complex $\lambda_\pm$, see (2.26). In the case of $h_1 = 1$ and $h_2 = 5$, E_c is calculated to be $2\left(\sqrt{5}-1\right)$. In Fig. 3.3 - 3.4 we give the examples of present investigation: $E = 2 < E_c$ in the case of Fig. 3.3 and $E = 4 > E_c$ in Fig. 3.4. Hence, we can observe the situation that the equilibrium solution is lost, if the total energy E is larger than critical energy E_c defined by helicities h_1 and h_2, when larger length scale is decreased to some critical value (defined by initial and boundary conditions) - when the specific deformation (or distortion) of initial structure is achieved for given case.

Let us now study the process at the critical point $\lambda_+ = \lambda_+^{\rm crit}$. Taking the derivative of (3.19) we find that $\mathrm{d}\lambda_+/\mathrm{d}\lambda_- = 0$, if

$$\left(1 \mp \frac{(\lambda_+ - \lambda_-)}{\sqrt{(\lambda_+ - \lambda_-)^2 + 4}}\right) E - 2\lambda_+ h_1 = 0. \tag{3.33}$$

Using the relation

$$\left(1 \mp \frac{(\lambda_+ - \lambda_-)}{\sqrt{(\lambda_+ - \lambda_-)^2 + 4}}\right)^{-1} = \frac{1}{4}\left[(\lambda_+ - \lambda_-)^2 + 4 \pm (\lambda_+ - \lambda_-)\sqrt{(\lambda_+ - \lambda_-)^2 + 4}\right], \quad (3.34)$$

the equation (3.33) may be written as

$$E - \frac{\lambda_+ h_1}{2}\left[(\lambda_+ - \lambda_-)^2 + 4 \pm (\lambda_+ - \lambda_-)\sqrt{(\lambda_+ - \lambda_-)^2 + 4}\right] = 0, \quad (3.35)$$

which, using (3.22), gives precisely the condition for C_- to be 0;

$$\begin{aligned} C_-^2 &\propto E - \left[1 + (\lambda_+ + \tilde{a})^2\right]\lambda_+ h_1 \\ &= E - \frac{\lambda_+ h_1}{2}\left[(\lambda_+ - \lambda_-)^2 + 4 \pm (\lambda_+ - \lambda_-)\sqrt{(\lambda_+ - \lambda_-)^2 + 4}\right] \\ &= 0. \end{aligned} \quad (3.36)$$

It means that, at the critical point, the equilibrium solution has $C_- = 0$, i.e., it is expressed by the single Beltrami field, that is, $\boldsymbol{B} = C_+\boldsymbol{G}_+$ ($\nabla \times \boldsymbol{B} = \lambda_+ \boldsymbol{B}$) with $\boldsymbol{V}$ parallel to $\boldsymbol{B}$. The behaviors of magnetic energy and flow kinetic energy for this case are plotted in Fig. 3.5. This figure shows that the magnetic energy reaches its minimum at the critical point. Hence, the magnetic energy is transfered to the flow when a magnetic field is deduced to a single Beltrami field. The latter is a more relaxed state (see Fig. 2.1).

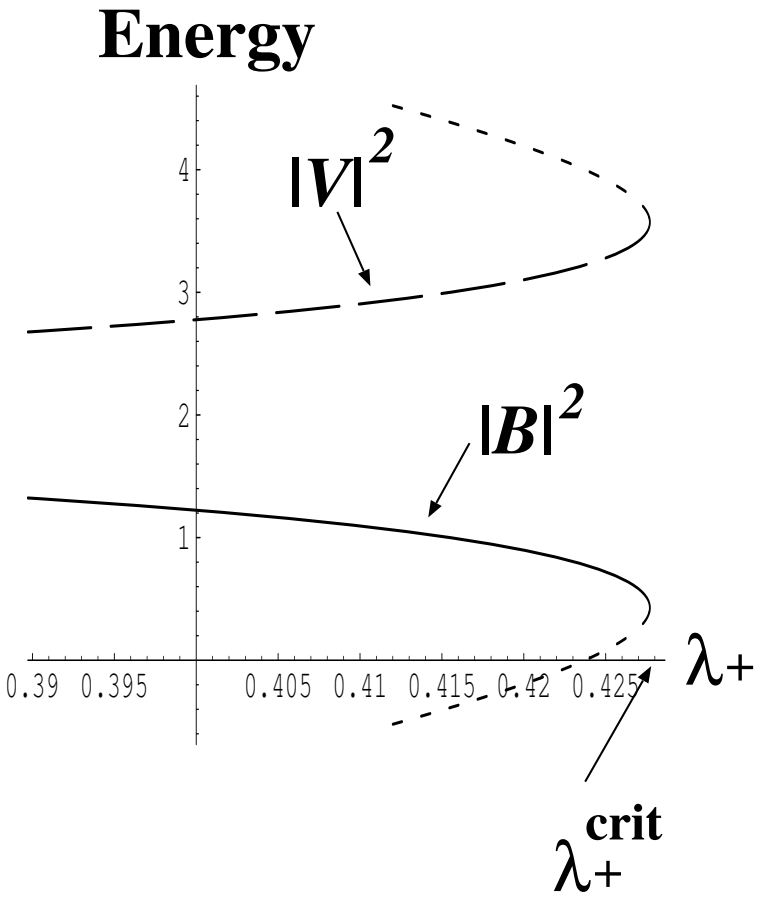

Figure 3.5: Energy of magnetic field and flow in the case of $E = 4 > E_c$.

3.5 Application to the solar corona

When applying the present model to the solar corona, we can find the conditions for coronal structure heating via magnetic field energy or even for the formation of eruptive events. If we consider λ_+ to be small such as $|\lambda_+| \ll |\lambda_-|$, i.e., we choose a very large scale ($|\lambda_+^{-1}|$) Beltrami field superposed by a small scale ($|\lambda_-^{-1}|$) one, then simple estimations give that $C_+ \sim O(\lambda_+/\lambda_-) \ll 1$ and $C_- \sim O(\lambda_-/\lambda_-) \sim 1$ from (3.21) and (3.22). However, when structures come into the interaction, it may happen that λ_+ starts to increase (the distortion or deformation process) and can reach a critical point ($\lambda_+ \stackrel{\rightarrow}{=} \lambda_+^{\text{crit}}$), and C_- becomes zero. Hence, magnetic field energy [$\propto (C_+^2 + C_-^2)$] decreases to a very small values since $C_+^2 \ll 1$. The total energy is still conserved. This implies that almost all the magnetic field energy can be transfered to the flow and as a result this energy can be transformed to heat the structure [46] or to create the eruptive events suddenly.

The Fig. 3.6 reproduces the case with the specific coronal structure parameters as $h_1 = 1$, $h_2 = 1.004$ and $E = 4$. For coronal plasma the ion skin depth l_i is $\sim$ 10m, then, macroscale of structure is $l_i/\lambda_+ \sim 10^4$(km) in this case - rather characteristic for corona.

Results found from this model show that, if in the dynamical process of hot coronal structure creation (see [46]) or structure-structure interactions plasma flows are treated properly, the coupling of magnetic and fluid aspects of the plasma provide the conditions for loss of equilibrium to end up creating eruptive events. In this case the appropriate sudden increase of λ_+ is required for the structures with certain helicities and energy.

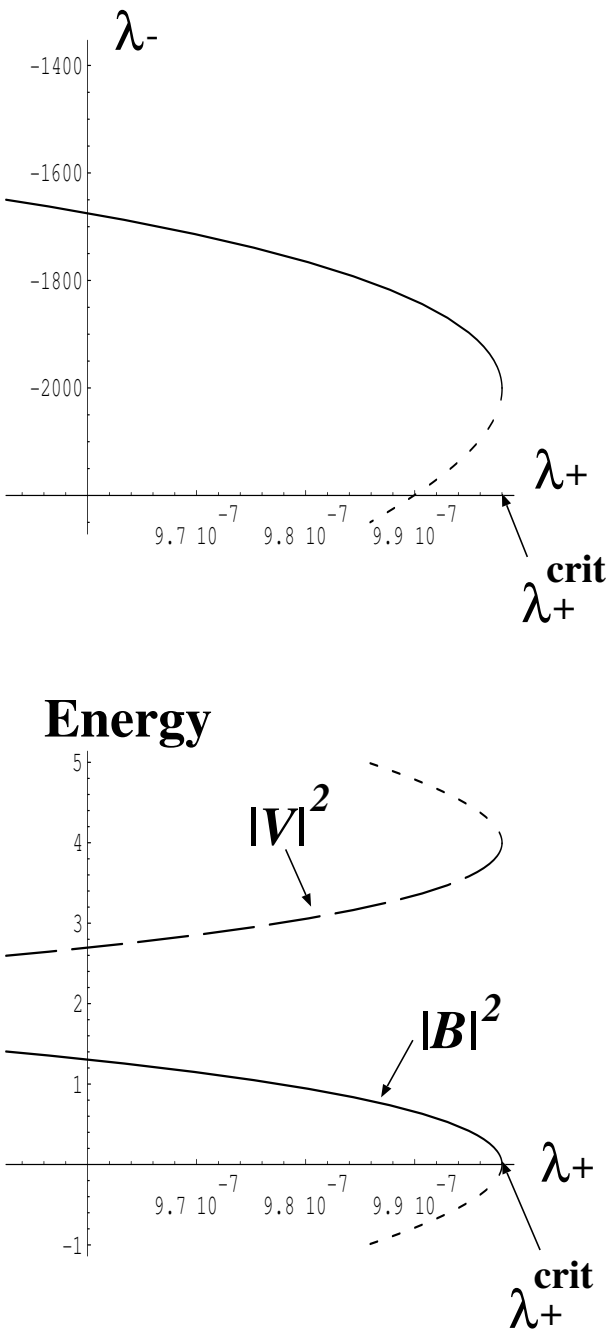

Figure 3.6: Behavior of λ_- and magnetic and flow energy in the large scale case.

Chapter 4

High-beta toroidal equilibrium in relaxed state with plasma flow

4.1 Introduction

Recently, in experimental and theoretical research of nuclear fusions, plasma flows in toroidal plasmas have attracted much attention. Theoretical studies of flowing plasmas begin in the mid-1950s, but most investigations of the equilibrium with plasma flow have done since the early 1970s ([29] and the references

therein). Toroidal flows can be driven by Neutral Beam Injection (NBI) [54] and poloidal flows by radial electric fields [55]. It has been reported that flow shear can reduce macro- and microscopic instabilities of plasmas [56, 57].

In this chapter, we treat a toroidal equilibrium of flowing plasmas as a relaxed state expressed by the double Beltrami equilibrium. As mentioned in Sec. 2.5, the generalized Bernoulli condition, implying that the energy density of the field is fully relaxed, gives a simple relation among the flow velocity, potential and the static pressure, that is, the plasma flow which is comparable to the Alfvén speed can produce a high-beta equilibrium where the plasma pressure is primarily balanced by the dynamic pressure of the flow. In order to invoke this effect, one must supply a driving force to induce and sustain the flow. One possible method to generate such a large flow is to introduce an appreciable charge non-neutrality that drives the $\boldsymbol{E} \times \boldsymbol{B}$ drift spin [31]. On the other hand, a steep gradient in pressure can leads this effect, too. This concept was applied to the H-mode boundary layer where a diamagnetic structure is self-organized with producing a coupling of the magnetic field, flow, electric field and pressure [36].

Considering an axisymmetric toroidal system, we can use the Clebsch representations for expressing the magnetic- and velocity field. Substituting these

expressions into the double Beltrami condition, a coupled Grad-Shafranov equation is derived in Sec. 4.2. A numerical method to the coupled Grad-Shafranov equation is discussed in Sec. 4.3, where we compare our numerical solution in large aspect ratio toroidal geometry with an analytical solution in cylindrical geometry for the confirmation of the correctness of our code. Next, since there is a fear that a high speed flow create a shock in this equilibrium, we try to examine the shock formation. Therefore, we give a concise review of the standard theory of MHD shocks in Sec. 4.4, and discuss the high-beta toroidal equilibrium with flow and the shock formation in this equilibrium in Sec. 4.5.

4.2 Formulation of coupled Grad-Shafranov equation

Due to the simple mathematical structure of the double Beltrami fields, it is rather easy to find analytical solutions of various equilibria in slab or cylindrical geometry. By choosing an appropriate set of parameters, we can construct very high beta solutions with producing a large flow velocity $\boldsymbol{V}$.

In this section, we present a coupled Grad-Shafranov equation of the dou-

ble Beltrami equilibrium. We consider axisymmetric two-dimensional equilibria. Following the basic idea of formulating the Grad-Shafranov equation, we use the Clebsch representations of divergence-free axisymmetric ($\partial_\theta = 0$) vector function in cylindrical (r, θ, z) coordinates [35]. We write $\boldsymbol{B}$ and $\boldsymbol{V}$ in a contravariant-covariant combination form

$$\boldsymbol{B} = \nabla\Psi(r,z) \times \nabla\theta + rB_\theta(r,z)\,\nabla\theta, \tag{4.1}$$

$$\boldsymbol{V} = \nabla\Phi(r,z) \times \nabla\theta + rV_\theta(r,z)\,\nabla\theta, \tag{4.2}$$

where Ψ (or Φ) is the flux function (or the stream function) of r and z, and B_θ (or V_θ) is the azimuthal magnetic (or velocity) field depending on r and z. We have

$$\nabla \times \boldsymbol{B} = \nabla(rB_\theta) \times \nabla\theta + \mathcal{L}\Psi\nabla\theta, \tag{4.3}$$

$$\nabla \times \boldsymbol{V} = \nabla(rV_\theta) \times \nabla\theta + \mathcal{L}\Phi\nabla\theta, \tag{4.4}$$

where $\mathcal{L}$ is the familiar Grad-Shafranov operator,

$$-\mathcal{L} = r\frac{\partial}{\partial r}\left(\frac{1}{r}\frac{\partial}{\partial r}\right) + \frac{\partial^2}{\partial z^2}. \tag{4.5}$$

Using these expressions in the double Beltrami condition (2.22) and (2.23), we

obtain

$$\begin{aligned}(\nabla\Phi\times\nabla\theta+rV_\theta\,\nabla\theta)-(\nabla(rB_\theta)\times\nabla\theta+\mathcal{L}\Psi\nabla\theta)\\ =\tilde{a}\,(\nabla\Psi\times\nabla\theta+rB_\theta\,\nabla\theta)\,,\\ (\nabla\Psi\times\nabla\theta+rB_\theta\,\nabla\theta)+(\nabla(rV_\theta)\times\nabla\theta+\mathcal{L}\Phi\nabla\theta)\\ =b\,(\nabla\Phi\times\nabla\theta+rV_\theta\,\nabla\theta)\,,\end{aligned}\tag{4.6}$$

where $\tilde{a}=1/a$. Summarizing (4.6) in the following form, and comparing each component

$$\begin{aligned}&\underbrace{\nabla(\Phi-rB_\theta-\tilde{a}\Psi)}_{=0}\times\nabla\theta+(\underbrace{rV_\theta-\mathcal{L}\Psi-\tilde{a}rB_\theta}_{=0})\nabla\theta=0,\\ &\underbrace{\nabla(\Psi+rV_\theta-b\Phi)}_{=0}\times\nabla\theta+(\underbrace{rB_\theta+\mathcal{L}\Phi-brV_\theta}_{=0})\nabla\theta=0,\end{aligned}\tag{4.7}$$

we get

$$\begin{cases}\Phi-rB_\theta-\Psi=C_1,\quad rV_\theta-\mathcal{L}\Psi-\tilde{a}rB_\theta=0,\\ \Psi+rV_\theta-b\Phi=C_2,\quad rB_\theta+\mathcal{L}\Phi-brV_\theta=0,\end{cases}\tag{4.8}$$

where C_1 and C_2 are constants to be determined by boundary (or flux) conditions. Then the double curl Beltrami equation translates as a following coupled Grad-Shafranov equation;

$$-\mathcal{L}\begin{pmatrix}\Psi\\ \\ \Phi\end{pmatrix}=\begin{pmatrix}1-\tilde{a}^2 & \tilde{a}-b\\ \\ b-\tilde{a} & 1-b^2\end{pmatrix}\begin{pmatrix}\Psi\\ \\ \Phi\end{pmatrix}-\begin{pmatrix}\tilde{a}C_1+C_2\\ \\ C_1+bC_2\end{pmatrix},\tag{4.9}$$

and

$$\begin{cases}rB_\theta=-\tilde{a}\Psi+\Phi-C_1,\\ rV_\theta=b\Phi-\Psi+C_2.\end{cases}\tag{4.10}$$

The coupled Grad-Shafranov equation of the type (4.9) was derived previously for the analysis of toroidal equilibrium in a plasma-beam system, where the inertia force of the beam particles brings about coupling of the magnetic field and the beam flow [58].

We note that the "vacuum fields" satisfying

$$-\mathcal{L}\Psi_v = 0, \tag{4.11}$$

$$-\mathcal{L}\Phi_v = 0, \tag{4.12}$$

can be included both in Ψ and Φ as inhomogeneous terms. Choosing appropriate vacuum fields, we can control the radial position and the shape of the toroidal equilibrium. Now, Ψ and Φ are decomposed as follows,

$$\Psi = \Psi_p + \Psi_v, \tag{4.13}$$

$$\Phi = \Phi_p + \Phi_v, \tag{4.14}$$

where Ψ_p and Φ_p are caused by the plasma current and the plasma flow vorticity. Then, (4.9) becomes

$$-\mathcal{L}\begin{pmatrix} \Psi_p \\ \Phi_p \end{pmatrix} = \begin{pmatrix} 1-\tilde{a}^2 & \tilde{a}-b \\ b-\tilde{a} & 1-b^2 \end{pmatrix}\begin{pmatrix} \Psi_p+\Psi_v \\ \Phi_p+\Phi_v \end{pmatrix} - \begin{pmatrix} \tilde{a}C_1+C_2 \\ C_1+bC_2 \end{pmatrix}. \tag{4.15}$$

4.3 Numerical analysis of Double Beltrami equilibrium

4.3.1 Algorithm of calculation

First, we have to mention a boundary condition, which determines the constants C_1 and C_2. Functions Ψ and Φ are biased to be $\Psi = 0$ and $\Phi = 0$ at the plasma boundary, and the plasma region is defined $\Psi > 0$ and $\Phi > 0$. Therefore we need to select the vacuum fields Ψ_v and Φ_v so that the regions of $\Psi > 0$ and $\Phi > 0$ coincide. We set the following boundary conditions to obtain free-boundary equilibria. A conductive vessel is not considered, so that Ψ and Φ go to constants at infinity. These constants are chosen so that $\Psi = 0$ and $\Phi = 0$ at the plasma boundary, which are defined by the contour of Ψ and Φ that touch the limiter, viz,

$$\max_{(r,z)\in\text{limiter}} \Psi(r,z) = 0, \tag{4.16}$$

$$\max_{(r,z)\in\text{limiter}} \Phi(r,z) = 0. \tag{4.17}$$

Solutions to toroidal double Beltrami equilibria are obtained by iterating numerical analyses of (4.15) in the following way. Letting Ψ_0 and Φ_0 satisfy

(4.15) with $C_1 = C_2 = 0$;

$$-\mathcal{L}\begin{pmatrix} \Psi_0 \\ \\ \Phi_0 \end{pmatrix} = \begin{pmatrix} 1-\tilde{a}^2 & \tilde{a}-b \\ \\ b-\tilde{a} & 1-b^2 \end{pmatrix}\begin{pmatrix} \Psi_0 \\ \\ \Phi_0 \end{pmatrix}, \tag{4.18}$$

we obtain a solution by finding functions $\Psi_0^{(n+1)}$ and $\Phi_0^{(n+1)}$ that satisfy the following equation with $\Psi_0^{(n+1)} = \Psi_0^{(n)}$ and $\Phi_0^{(n+1)} = \Phi_0^{(n)}$:

$$\begin{pmatrix} \Psi_0^{(n+1)} \\ \\ \Phi_0^{(n+1)} \end{pmatrix} = (-\mathcal{L})^{-1}\left[\begin{pmatrix} 1-\tilde{a}^2 & \tilde{a}-b \\ \\ b-\tilde{a} & 1-b^2 \end{pmatrix}\begin{pmatrix} \Psi_0^{(n)} \\ \\ \Phi_0^{(n)} \end{pmatrix}\right] + \begin{pmatrix} \Psi_v^{(n+1)} \\ \\ \Phi_v^{(n+1)} \end{pmatrix}, \tag{4.19}$$

where $(-\mathcal{L})^{-1}$ is calculated by

$$(-\mathcal{L})^{-1} F(r,z) = \int G(r,z,r',z')\frac{F(r',z')}{r'}\mathrm{d}r'\mathrm{d}z', \tag{4.20}$$

and

$$G(r,z,r',z') = \frac{1}{\pi\kappa}(rr')^{1/2}\left[\left(1-\frac{\kappa^2}{2}\right)K(\kappa) - E(\kappa)\right], \tag{4.21}$$

$$\kappa^2 = \frac{4rr'}{(r+r')^2 + (z-z')}. \tag{4.22}$$

Here, $K(\kappa)$ and $E(\kappa)$ are complete elliptic integrals of the first and second kind, respectively. We note that $F(r',z')/r'$ in (4.20) corresponds to the toroidal current density, $(\nabla \times \boldsymbol{B})_\theta$, and/or the toroidal vorticity, $(\nabla \times \boldsymbol{V})_\theta$, in this system.

Using Ψ_0 and Φ_0, we get Ψ and Φ, which satisfy the boundary conditions (4.16) and (4.17),as follows

$$\Psi(r,z) = \Psi_0(r,z) - \Psi_b, \tag{4.23}$$

$$\Phi(r,z) = \Phi_0(r,z) - \Phi_b, \tag{4.24}$$

where

$$\max_{(r,z)\in\text{limiter}} \Psi(r,z) = \Psi_b, \qquad \max_{(r,z)\in\text{limiter}} \Phi(r,z) = \Phi_b. \tag{4.25}$$

Substituting (4.23) and (4.24) into (4.9) or (4.15), we get

$$\begin{pmatrix} 1-\tilde{a}^2 & \tilde{a}-b \\ b-\tilde{a} & 1-b^2 \end{pmatrix} \begin{pmatrix} \Psi_b \\ \Phi_b \end{pmatrix} + \begin{pmatrix} \tilde{a}C_1 + C_2 \\ C_1 + bC_2 \end{pmatrix} = 0, \tag{4.26}$$

and so the constants C_1 and C_2 are given by the boundary conditions as follows

$$C_1 = \tilde{a}\Psi_b - \Phi_b, \quad C_2 = -\Psi_b + b\Phi_b. \tag{4.27}$$

Furthermore, substituting (4.23) and (4.24) into (4.10), we get

$$\begin{cases} rB_\theta = -\tilde{a}\Psi_0 + \Phi_0, \\ rV_\theta = b\Phi_0 - \Psi_0, \end{cases} \tag{4.28}$$

which insist that physical quantities are independent of 0-point (bias) of potentials Ψ and Φ.

4.3.2 Comparison between analytical and numerical solutions

In the following calculations, we fix the toroidal plasma current and the total toroidal plasma vorticity as I_t and Ω_t;

$$\begin{aligned} I_t &= \int (\nabla \times \boldsymbol{B})_\theta \, \mathrm{d}S = \text{const}, \\ \Omega_t &= \int (\nabla \times \boldsymbol{V})_\theta \, \mathrm{d}S = \text{const}, \end{aligned} \tag{4.29}$$

where $\int \mathrm{d}S$ is an integration on the poloidal cross section. Under these conditions, we can calculate (4.19) easily in the case of $\tilde{a} = b$, because the coupled Grad-Shafranov equation is reduced to an eigen value problem:

$$-\mathcal{L} \begin{pmatrix} \Psi_0 \\ \\ \Phi_0 \end{pmatrix} = \left(1 - \tilde{a}^2\right) \begin{pmatrix} \Psi_0 \\ \\ \Phi_0 \end{pmatrix}, \tag{4.30}$$

and

$$\Phi_0 = \frac{\Omega_t}{I_t} \Psi_0. \tag{4.31}$$

Saying physically, the magnetic (velocity) field is expressed by a linear combination of two Beltrami fields, eigenvalues of which have opposite signs and same absolute values, that is, $\lambda_- = -\lambda_+$, see (2.26).

In this section, we compare a numerical solution to (4.30) in large aspect ratio with an analytical solution in cylindrical geometry for the confirmation of the correctness of our code (see Fig. 4.1).

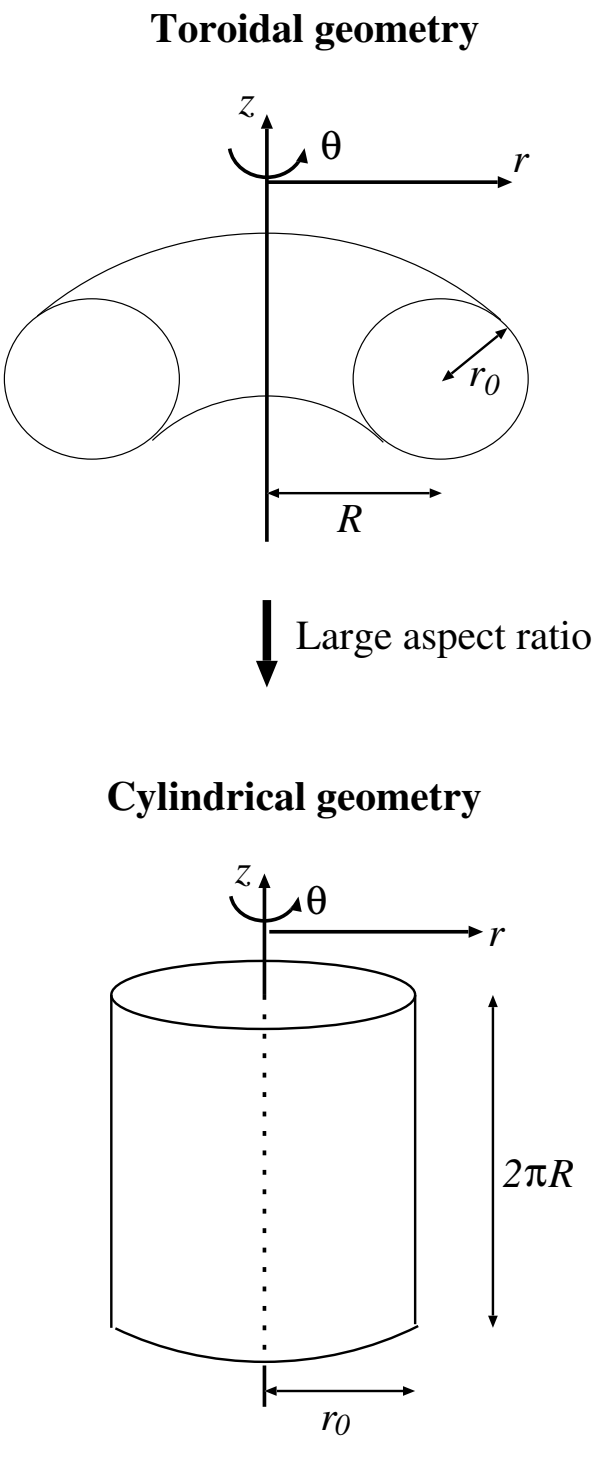

Figure 4.1: Comparison between toroidal and cylindrical geometry.

The Clebsch representations of cylindrical z-symmetry are given by

$$\boldsymbol{B} = \nabla\frac{\hat{\Psi}(r)}{R}\times\nabla z + B_z(r)\,\nabla z, \tag{4.32}$$

$$\boldsymbol{V} = \nabla\frac{\hat{\Phi}(r)}{R}\times\nabla z + V_z(r)\,\nabla z, \tag{4.33}$$

where R is a major radius corresponding to toroidal geometry (see Fig. 4.1). In the cylindrical system, for arbitrary constants $C_\pm$, the general solution of the double Beltrami equation is written by

$$\begin{cases} B_t = B_z = C_+ J_0(\lambda_+ r) + C_- J_0(\lambda_- r), \\ B_p = B_\theta = C_+ J_1(\lambda_+ r) + C_- J_1(\lambda_- r), \end{cases} \tag{4.34}$$

and

$$\begin{cases} V_t = V_z = (\tilde{a}+\lambda_+)\,C_+ J_0(\lambda_+ r) + (\tilde{a}+\lambda_-)\,C_- J_0(\lambda_- r), \\ V_p = V_\theta = \left[(\tilde{a}+\lambda_+)\,C_+ J_1(\lambda_+ r) + (\tilde{a}+\lambda_-)\,C_- J_1(\lambda_- r)\right], \end{cases} \tag{4.35}$$

where J_0 and J_1 are the ordinary Bessel functions and notation t (or p) expresses the toroidal (or poloidal) direction. Since, using (4.34) and (4.35), the constants I_t and Ω_t are given by

$$\begin{aligned} I_t &= 2\pi\int_0^{r_0}\frac{\partial}{\partial r}\left(rB_p\right)\mathrm{d}r \\ &= 2\pi\left[r_0 C_+ J_1(\lambda_+ r_0)\} + r_0 C_- J_1(\lambda_- r_0)\right], \end{aligned} \tag{4.36}$$

$$\begin{aligned} \Omega_t &= 2\pi\int_0^{r_0}\frac{\partial}{\partial r}\left(rV_p\right)\mathrm{d}r \\ &= 2\pi\left[(\tilde{a}+\lambda_+)\,r_0 C_+ J_1(\lambda_+ r_0)\} + (\tilde{a}+\lambda_-)\,r_0 C_- J_1(\lambda_- r_0)\right], \end{aligned} \tag{4.37}$$

we can obtain $C_\pm$ as

$$C_+ = \frac{\Omega_t - (\tilde{a} + \lambda_-)\, I_t}{2\pi r_0\, (\lambda_+ - \lambda_-)\, J_1(\lambda_+ r_0)}, \tag{4.38}$$

$$C_- = \frac{-\Omega_t + (\tilde{a} + \lambda_+)\, I_t}{2\pi r_0\, (\lambda_+ - \lambda_-)\, J_1(\lambda_- r_0)}, \tag{4.39}$$

where r_0 is a minor radius. Therefore, integrating (4.34) and (4.35) from 0 to r_0 with r and from 0 to $2\pi R$ with z, the corresponding $\hat{\Psi}$ and $\hat{\Phi}$ are calculated as

$$\hat{\Psi} = R\left[\frac{C_+}{\lambda_+}\{1 - J_0(\lambda_+ r)\} + \frac{C_-}{\lambda_-}\{1 - J_0(\lambda_- r)\}\right], \tag{4.40}$$

$$\hat{\Phi} = R\left[(\tilde{a} + \lambda_+)\frac{C_+}{\lambda_+}\{1 - J_0(\lambda_+ r)\} + (\tilde{a} + \lambda_-)\frac{C_-}{\lambda_-}\{1 - J_0(\lambda_- r)\}\right]. \tag{4.41}$$

We compare Ψ and Φ given by (4.23) and (4.24) with $\hat{\Psi}$ and $\hat{\Phi}$ in Fig. 4.2 - Fig. 4.3, where we set the aspect ratio is 100 ($r_0 = 1$ and $R = 100$). In this case, $\lambda_\pm$, which are eigenvalues of two Beltrami fields, are given ± 0.738 ($\tilde{a} = b = 1.243$). We calculate two cases of Ψ and Φ. The first one is $I_t = 3.0$ and $\Omega_t = 4.0$, which is plotted in Fig. 4.2, the second one is $I_t = 3.0$ and $\Omega_t = 5.0$ in Fig. 4.3. In these figures, the numerical solution Ψ (or Φ) is expressed by a point $\times$ (or $+$), and analytical solution $\hat{\Psi}$ (or $\hat{\Phi}$) is drawn by a solid (or dashed) line. We can ascertain that the numerical and the analytical

solutions coincide well. Not only in these cases but also in other ones, the numerical solutions to large aspect ratio agree well with the analytical solutions given by (4.40) and (4.41).

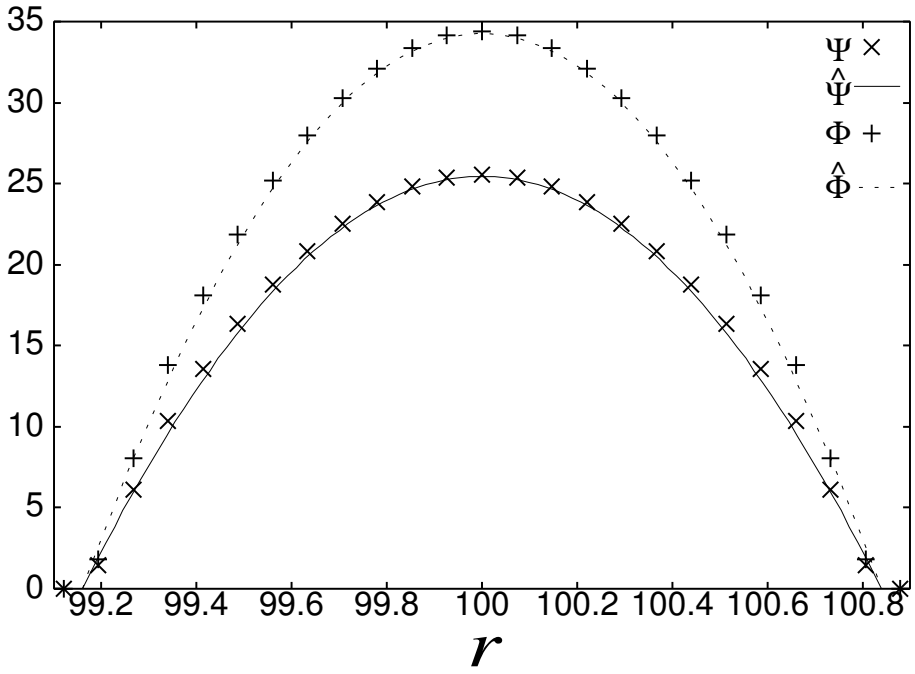

Figure 4.2: Comparison between numerical and analytical solution in the case of $I_t = 3.0$ and $\Omega_t = 4.0$.

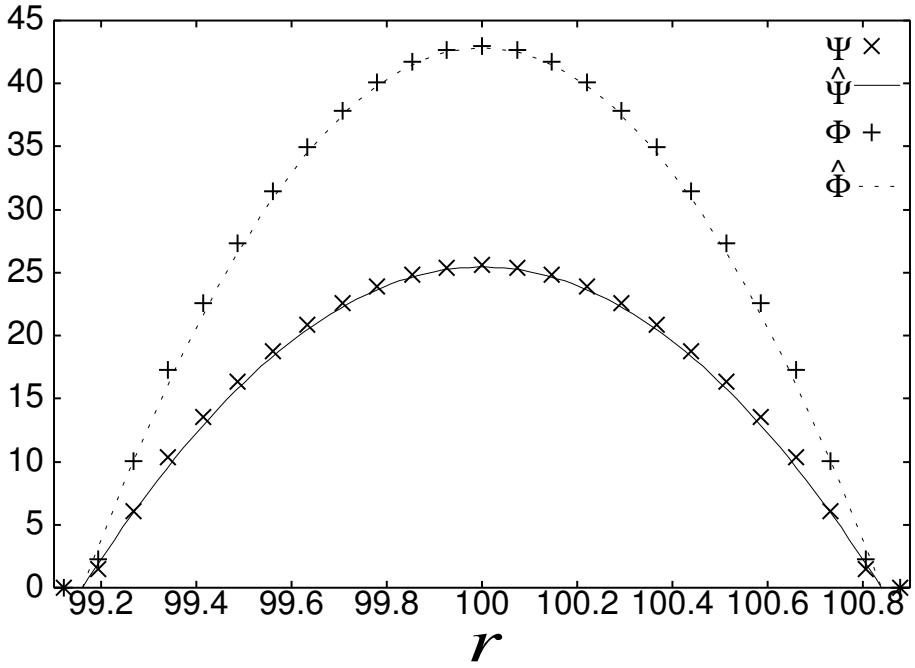

Figure 4.3: Comparison between numerical and analytical solution in the case of $I_t = 3.0$ and $\Omega_t = 5.0$.

4.4 Shock conditions for plasma flow

Using a shock condition for one-fluid MHD (evolutionary condition), we will discuss a local shock condition for the double Beltrami equilibrium in toroidal system. Here "local" means that it is a small region such that we can treat field lines of $\boldsymbol{B}$ and $\boldsymbol{V}$ as straight ones (Fig. 4.4). In this section, we give a concise review of the standard theory of MHD shocks, especially evolutionary shocks.

For MHD shocks, we invoke the evolutionary condition [59]-[61], which was applied to single Beltrami magnetic field's shocks [12]. This condition warrants the existence of a unique solution to the small-perturbation (linearized) problem. This is equivalent to demanding that the boundary condition given at the shock front can determine the all modes of waves created there together with the perturbation of the shock itself. This comes up to the criteria that a shock is evolutionary if the number of the outgoing waves is equal to the number of boundary conditions minus one (that corresponds to the perturbation of the shock). In order to ascertain the actual condition for shock waves to be evolutionary in an MHD plasma, let us first count the number of equations to be satisfied by any small perturbation at the discontinuity surface. The shock

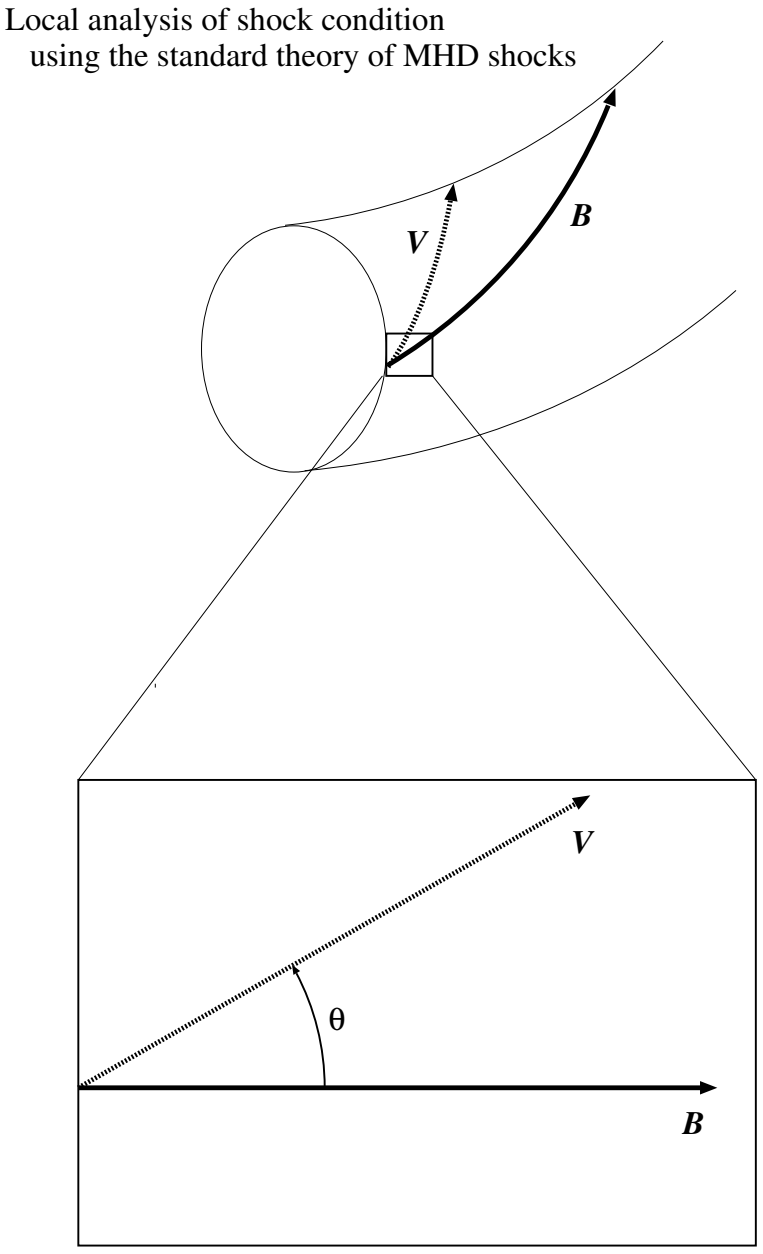

Figure 4.4: Local analysis.

will be regarded as lying in the y-z plane. The positive x direction is taken to be that of the flow across the discontinuity surface.

On each side of the shock, all quantities undergo perturbation. In addition, the speed of propagation of the shock wave itself is perturbed, i.e., it acquires a small velocity $\delta\boldsymbol{U} = \delta U \boldsymbol{e}_x$ (where $\boldsymbol{e}_x$ is a unit vector of x direction). We write $\boldsymbol{v} + \delta\boldsymbol{v} - \delta\boldsymbol{U}$, $\boldsymbol{B} + \delta\boldsymbol{B}$, $\rho + \delta\rho$, $p + \delta p$, where $\boldsymbol{v}$, $\boldsymbol{B}$, ρ and p are the unperturbed values; $\delta\boldsymbol{v}$, $\delta\boldsymbol{B}$, $\delta\rho$ and δp are the small perturbations.

Assuming all quantities to depend only on x and time t, and setting

$$\boldsymbol{B} = \begin{pmatrix} B_x \\ B_y \\ 0 \end{pmatrix}, \quad \boldsymbol{v} = \begin{pmatrix} v \\ 0 \\ 0 \end{pmatrix}, \quad \delta\boldsymbol{B} = \begin{pmatrix} 0 \\ \delta B_y \\ \delta B_z \end{pmatrix}, \quad \delta\boldsymbol{v} = \begin{pmatrix} \delta v_x \\ \delta v_y \\ \delta v_z \end{pmatrix},$$

we seek all perturbations in a form proportional to $\exp\{i(kx - \omega t)\}$. Substituting these conditions in MHD equations, we can get seven different phase velocities of linear waves (boundary conditions); two Alfvén waves ($v \pm V_{Ax}$), four magnetosonic waves (two fast waves $v \pm V_f$ and two slow waves $v \pm V_s$) and an entropy wave. Here,

$$V_{Ax} = V_A \cos\theta = \sqrt{\frac{B_x^2}{\rho\mu_0}}, \tag{4.42}$$

$$V_f = \left\{ (1/2) \left[V_A^2 + C_s^2 + \sqrt{\left(V_A^2 + C_s^2\right)^2 - 4V_{Ax}^2 C_s^2} \right] \right\}^{1/2}, \tag{4.43}$$

$$V_s = \left\{ (1/2) \left[V_A^2 + C_s^2 - \sqrt{\left(V_A^2 + C_s^2\right)^2 - 4V_{Ax}^2 C_s^2} \right] \right\}^{1/2}, \qquad (4.44)$$

where V_A is the Alfvén velocity, C_s is the sound velocity and θ is the angle between the background flow (i.e., x-direction) and magnetic field. The V_{Ax} is the x-component of the Alfvén velocity.

Since the number of boundary conditions is 7, a shock is evolutionary when the number of outgoing waves is $7 - 1 = 6$. However, mere equality of the number of equations to the number of unknowns is insufficient for the existence and uniqueness of the solution. For MHD, the equations for the amplitudes of the outgoing waves and boundary conditions break up into two isolated groups. In this case, the evolutionary conditions must be satisfied not only for the totality of the variables, but also for each group separately. In fact, in Alfvén waves the quantities δB_z and δv_z differ from zero, while in magnetosonic and entropy waves $\delta\rho$, δB_y, δv_x and δv_y differ from zero. The boundary conditions, linearized relative to small perturbations, also break up into similar two groups:

- Alfvén waves

$$\begin{cases} (v - v_{ph})\, \delta B_z - B_x \delta v_z = 0, \\ (v - v_{ph})\, \delta v_z - \frac{B_x}{\rho\mu_0} \delta B_z = 0. \end{cases} \qquad (4.45)$$

- Magnetosonic and entropy waves

$$\begin{cases} (v - v_{ph})\,\delta\rho + \rho\,(\delta v_x - \delta U) = 0, \\ (v - v_{ph})\,\delta B_y + B_y\,(\delta v_x - \delta U) - B_x \delta v_y = 0, \\ (v - v_{ph})\,(\delta v_x - \delta U) + \frac{1}{\rho}\delta p + \frac{B_y}{\rho\mu_0}\delta B_y = 0, \\ (v - v_{ph})\,\delta v_y - \frac{B_x}{\rho\mu_0}\delta B_y = 0, \\ (v - v_{ph})\,\delta p + \gamma p\,(\delta v_x - \delta U) = 0. \end{cases} \tag{4.46}$$

Here, $v_{ph} = \omega/k$. The boundary conditions (4.45) do not contain δU. They are, therefore, all independent and there should be two outgoing Alfvén waves. The boundary conditions (4.46) contain the perturbation δU of the shock wave velocity, after this perturbation is eliminated, four independent boundary conditions remain. Consequently, the number of outgoing magnetosonic and entropy waves should be four. Therefore, we must have two Alfvén waves and four other waves consisting the total six outgoing waves.

The phase velocities of the linear waves in both regions are

$$\begin{cases} v_{ph1} = v_1, v_1 \pm V_{Ax1}, v_1 \pm V_{f1}, v_1 \pm V_{s1}, \\ v_{ph2} = v_2, v_2 \pm V_{Ax2}, v_2 \pm V_{f2}, v_2 \pm V_{s2}. \end{cases}$$

For the wave to be outgoing, it must have a negative phase velocity in the region-1 ($v_{ph1} < 0$) and a positive phase velocity in the region-2 ($v_{ph2} > 0$), see Fig. 4.5 (a). Then, there exist two regions (correspond to fast and slow shock

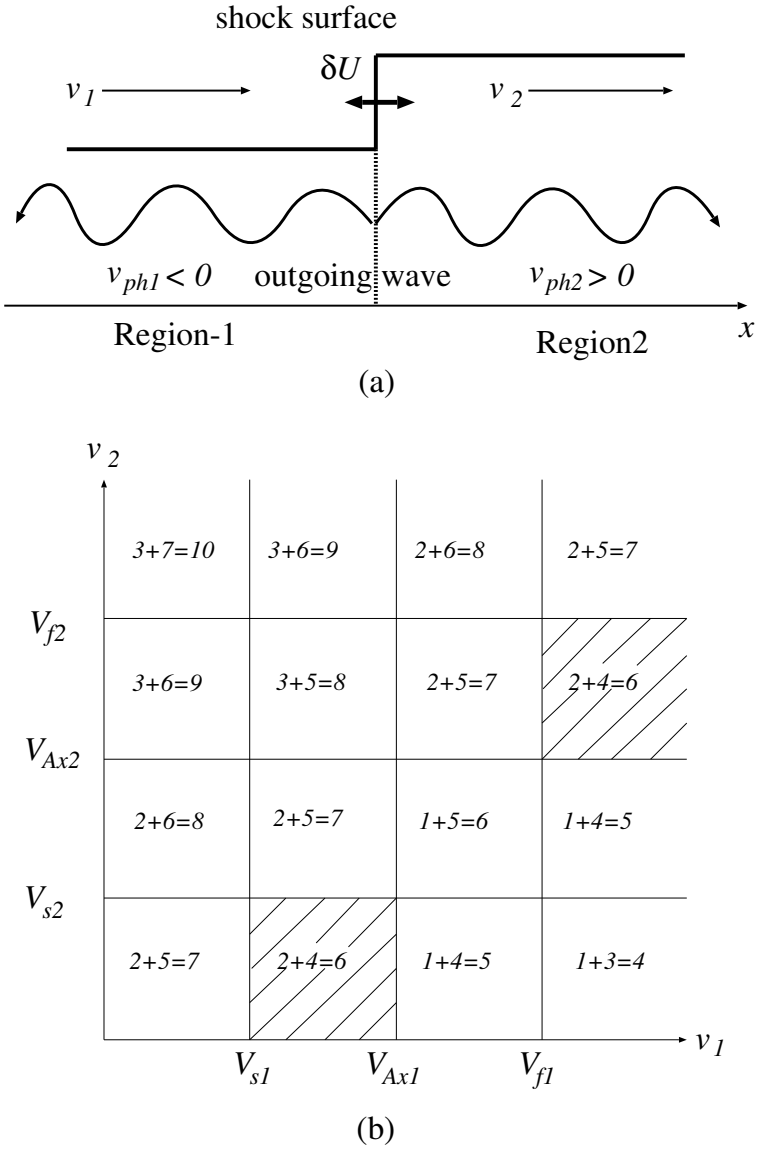

Figure 4.5: (a) Outgoing waves in Region-1 and -2, (b) Diagram for outgoing waves.

waves) where the shock waves are evolutionary. That is, a region of $V_{f1} < v_1$, $V_{Ax2} < v_2 < V_{f2}$ gives the fast shock waves, and a region of $V_{s1} < v_1 < V_{Ax1}$, $v_2 < V_{s2}$ gives the slow shock waves; the shaded regions in Fig. 4.5 (b).

4.5 Result and discussion

Finally, we discuss an equilibrium with plasma flow in small aspect ratio toroidal geometry. Setting the aspect ratio is 3 ($R = 3.0$, $r_0 = 1.0$), we solve the basic equations (4.9) and (4.10). In this case, $\lambda_\pm$ are given by ± 1.47 ($\tilde{a} = b = 1.78$). The results are shown in Fig. 4.6 - Fig. 4.7; we plot the contour of Ψ and Φ in Fig. 4.6, β profile and contour in Fig. 4.7, where we choose $I_t = 3.5$ and $\Omega = 2.5$. In this equilibrium, the beta ratio can be achieved $\sim 30\%$, but there is an undesirable jump of pressure at the plasma edge.

Next, using evolutionary condition, we examine a local shock formation in this case. Here, we think naively, if the plasma flow velocity $V = |\boldsymbol{V}|$ is larger than V_s and smaller than V_{Ax}, the slow shock may be created, and if $V_f < V$, the fast shock may appear. For reference, we show the phase polars in Fig 4.8, where each curve depicts the each wave's dependence on the angle θ between the direction of the plasma flow and the direction of the magnetic field; see

(4.42) - (4.44). We plot the plasma flow $|\boldsymbol{V}|$ and local V_s, V_{Ax} and V_f at each point in Fig. 4.9. This figure indicates that the plasma flow can create a slow shock in hatched region.

Now, we have two problems to be solved.

(i) There is a jump of beta (pressure) at the boundary of plasma.

(ii) There is a possibility that a slow shock is created in the plasma.

The statement of (i) is that there is a steep gradient in pressure, which can leads a self-organized shear-flow layer like a H-mode boundary layer [36]. Then, having an optimistic view, there is a possibility to keep a high-beta equilibrium, but it is a very important problem that have been left unsolved. On the other hand, we may solve (ii) easily by setting the Beltrami parameters $\tilde{a}$ and b as proper values. In our code, at present time, we calculate only the case of $\tilde{a} = b$. We show two analytical results calculated in cylindrical geometry using the solutions (4.34) and (4.35) in Fig. 4.10 and Fig. 4.11, where we set $\tilde{a} = -1$, $b = 0.5$ and $\tilde{a} = -1$, $b = 1$ respectively. In both figures, the beta profile are plotted in (a), the flow profile in (b). From these results, we can say that a high-beta equilibrium can exist avoiding a shock or minimizing this effect. Then we believe that we can achieve a high-beta toroidal equilibrium without

shock by setting proper $\tilde{a}$ and b.

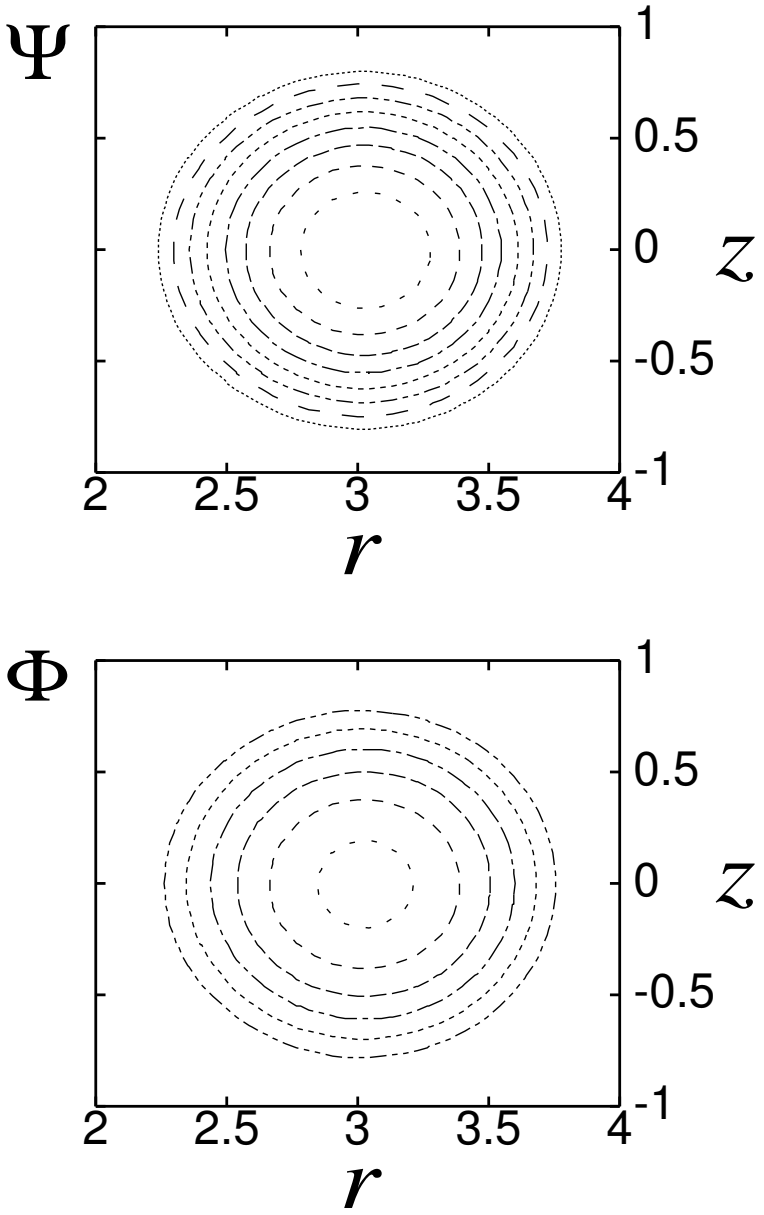

Figure 4.6: The contours of Ψ and Φ in toroidal equilibrium of high-beta double Beltrami field.

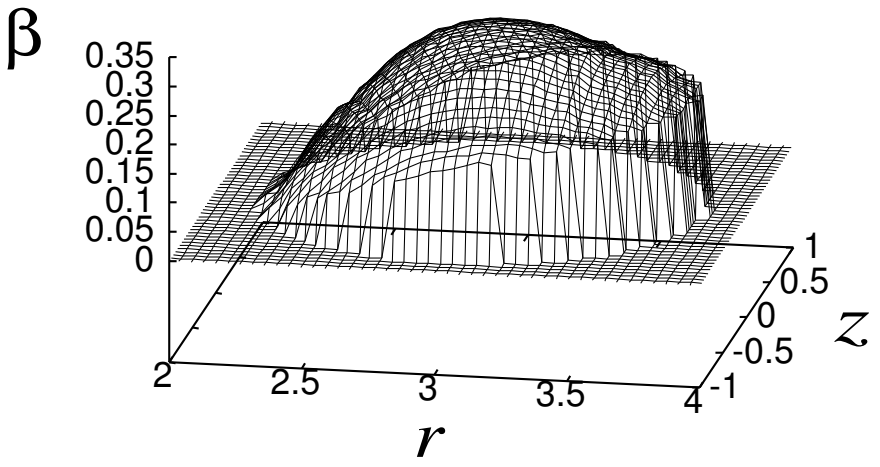

(a)

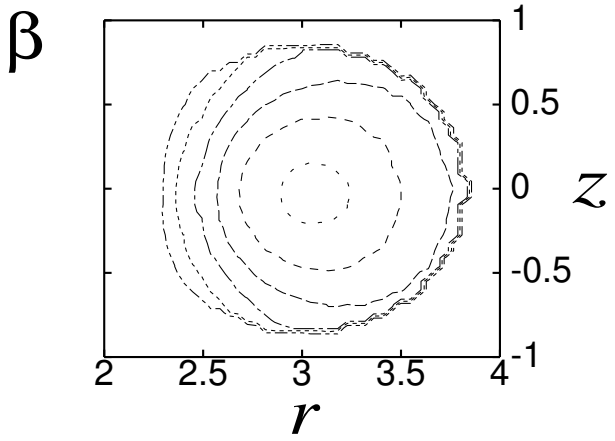

(b)

Figure 4.7: The beta profile and contour in toroidal equilibrium of high-beta double Beltrami field.

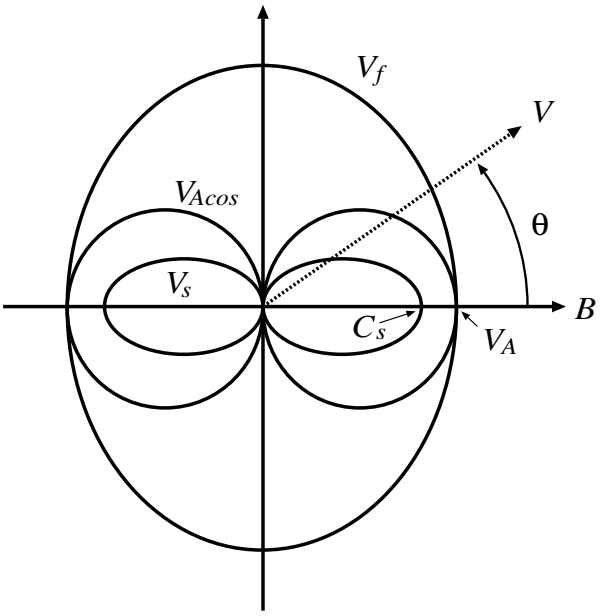

(a) $V_A > C_s$

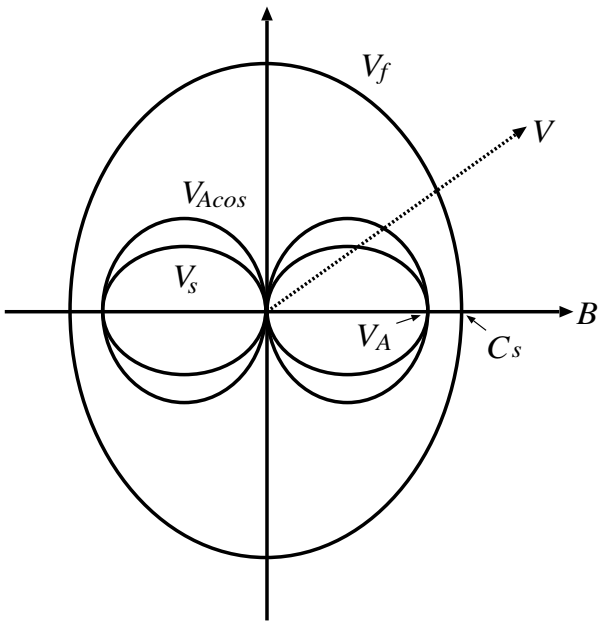

(b) $V_A < C_s$

Figure 4.8: Phase polars (a) $V_A > C_s$, (b) $V_A < C_s$.

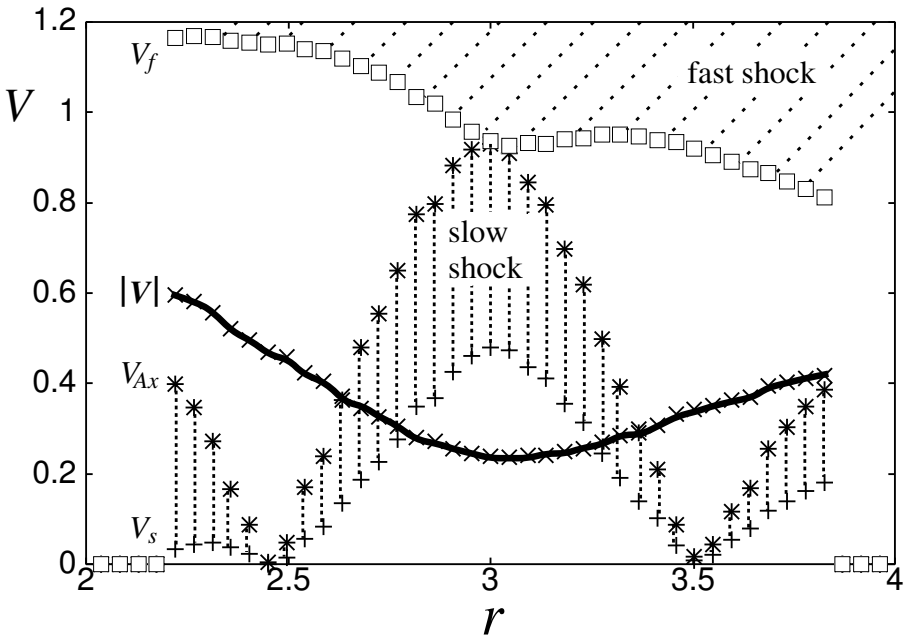

Figure 4.9: Plasma flow and the regions of shock formation in toroidal equilibrium of high-beta double Beltrami field.

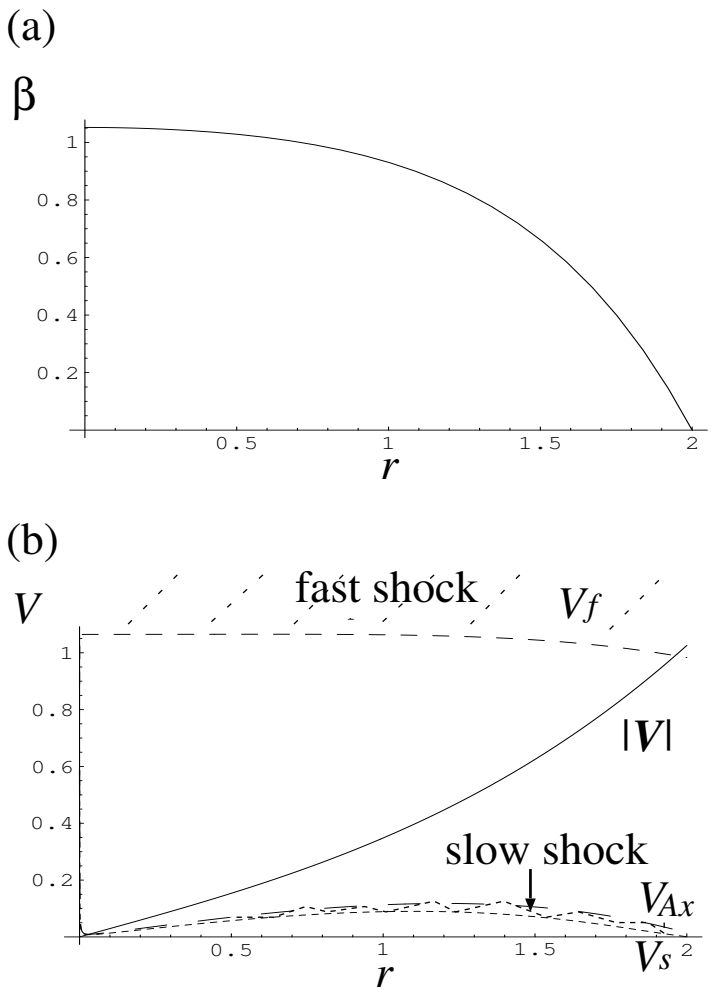

Figure 4.10: Plasma flow and the regions of shock formation in cylindrical equilibrium of high-beta double Beltrami field when $\tilde{a} = -1$, $b = 0.5$.

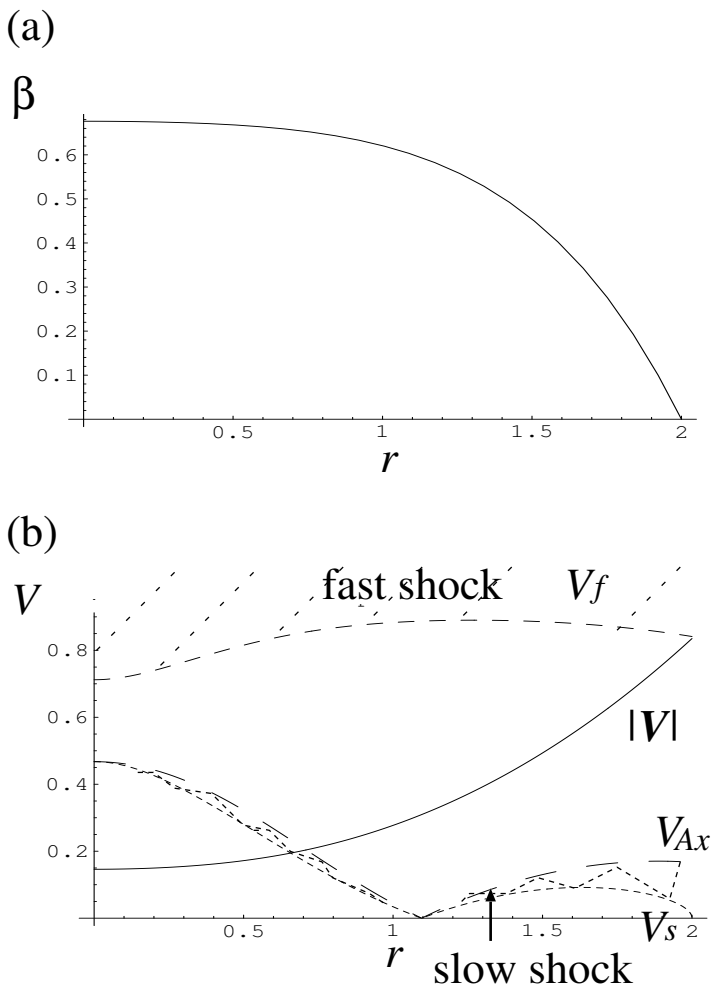

Figure 4.11: Plasma flow and the regions of shock formation in cylindrical equilibrium of high-beta double Beltrami field when $\tilde{a} = -1$, $b = 1$.

Chapter 5

Summary

The two-fluid model of a plasma describes the strong coupling between the magnetic and the fluid aspects of the plasma. The Beltrami condition which demands alignment of vortices and flows reads as a system of simultaneous equations for the magnetic field and the flow velocity. Combination of these equations yields the double curl Beltrami equation where the magnetic field and the velocity field are self-consistently coupled. The set of solutions called double Beltrami fields describe field configurations which can be qualitatively different from the conventional single Beltrami fields (Taylor relaxed states). By virtue of the double Beltrami fields, the flow effect can be introduced to relaxed plasma states. The larger new set may help us to understand a variety

of structures generated in plasmas.

A double Beltrami field is expressed by a linear combination of two different single Beltrami fields, and, hence, is characterized by four parameters (two eigenvalues and two amplitudes). In Chap. 3, relating these parameters with the macroscopic constants of motion (helicities and energy), we obtain an interesting set of algebraic relations, and discuss catastrophic behavior of equilibrium with respect to the change of the length scale. We find that, if the total energy is larger than critical energy, the equilibrium is lost when length scale is decreased. We suggest that at the critical length scale (where the loss of equilibrium occurs) a magnetic field is reduced to a single Beltrami field and its energy is minimized.

Next, considering a field with significant scale separation, we try to apply this model to the solar corona and get the result suggesting one of possible routes of solar eruptions as the loss of equilibrium. This event may occur owing to energy storage and the trigger of eruption is interacting coronal flux loops. Finally we show that a large amount of energy is transfered from the magnetic field to the flow.

The combination of two Beltrami fields yields a finite beta value, and hence, diamagnetic and high-beta structures are within the scope of the theory. The

generalized Bernoulli condition, implying that the energy density of the field is fully relaxed, gives a simple relation among the flow velocity, potential and the static pressure. When we drive a strong flow (in the Alfvén unit), very high-beta equilibrium can be obtained. In Chap. 4, in order to consider the double Beltrami states in toroidal geometry, using Clebsch potential Ψ (flux function) and Φ (stream function), a coupled Grad-Shafranov equation is derived. Solving this equation numerically, we show and discuss the high-beta toroidal equilibrium.

Next, we investigate a shock created by a high-speed plasma flow. Using the (one-fluid) MHD shock theory, we examine whether the plasma flow in equilibrium can avoid creating a shock or not. In this study, we think naively, if the plasma flow velocity is larger than the slow wave and smaller than the Alfvén wave's parallel component to the flow, the slow shock may be formed, and if the flow is larger than the fast wave, the fast shock may appear. According to the result of our calculation, where we can not find general equilibria but only a special case of the Beltrami parameters $\tilde{a} = b$, it is suggested that there is a possibility of a slow shock creation in a plasma. Analytical solutions in cylindrical geometry, however, indicate that we can get high-beta equilibria avoiding shock formations or making their effect small in the double Beltrami

states. Then we have to study toroidal equilibria on arbitrary Beltrami parameters $\tilde{a}$ and b, and get high-beta toroidal equilibria with plasma flow but without a shock.

Bibliography

[1] Z. Yoshida, in *Current Topics in the Physics of Fluids* (Council of Scientific Information, Trivandrum 1994), Vol. 1, p. 155-178.

[2] A. Hasegawa, Adv. Phys. **34**, 1 (1985).

[3] Z. Yoshida and Y. Giga, Math. Z. **204**, 235 (1990).

[4] For statistical mechanical treatments, see D. Montgomery, L. Turner, and G. Vahala, Phys. Fluids **21**, 757 (1978); N. Ito and Z. Yoshida, Phys. Rev. E **53**, 5200 (1996); R. Jordan, Z. Yoshida, and N. Ito, Physica D **114**, 251 (1998).

[5] J. B. Taylor, Phys. Rev. Lett. **33**, 1139 (1974).

[6] R. Lüst and A. Schlüter, Z. F. Ap. **34**, 263 (1954).

[7] S. Chandrasekhar, Proc. Nat. Acad. Sci. **42**, 1 (1956).

[8] S. Chandrasekhar and P.C. Kandall, Astrophys. J. **126**, 457 (1957).

[9] L. Acton, S. Tsuneta and Y. Ogawara *et al.*, Science **258**, 618 (1992).

[10] A. Königl and A.R. Choudhuri, Astrophys. J. **289**, 173 (1985).

[11] R. P. Lepping, L. F. Burlaga, A. Szabo *et al.*, J. Geophys. Res. **102**, 14049 (1997).

[12] S. Ohsaki and Z. Yoshida, Phys. Plasmas **7**, 2404 (2000).

[13] J. B. Taylor, Rev. Mod. Phys. **58**, 741 (1986).

[14] Z. Yoshida *et al.*, J. Plasma Phys. **59**, 103 (1998).

[15] S. M. Mahajan and Z. Yoshida, Phys. Rev. Lett. **81**, 4863 (1998).

[16] Z. Yoshida and S. M. Mahajan, J. Math. Phys. **40**, 5080 (1999).

[17] B. N. Handy, L. W. Acton, C. C. Kankelborg *et al.*, Solar Phys. **187**, 229 (1999).

[18] C. J. Schrijver, A. M. Title, T. E. Berger *et al.*, Solar Phys. **187**, 261 (1999).

[19] M. J. Aschwanden, T. D. Tarbell, R. W. Nightingale *et al.*, Astrophys. J. **535**, 1047 (2000); M. J. Aschwanden, Solar Phys. **190**, 233 (1999).

[20] L. Golub, J. Bookbinder, E. DeLuca *et al.*, Phys. Plasma **6**, 2205 (1999).

[21] J. L. Kohl, G. Noci, E. Antonucci *et al.*, Solar Phys. **175**, 613 (1997); X. Li, S. R. Habbal, J. L. Kohl, and G. Noci, Astrophys. J. **501**, L133 (1998).

[22] M. J. Aschwanden, D. Alexander, N. Hurlburt *et al.*, Astrophys. J. **531**, 1129 (2000); O. Kjeldeth-Moe and P. Brekke, Solar Phys. **182**, 73 (1998).

[23] J. M. Beckers, Ann. Rev. A&A **10**, 73 (1972); Astrophys. J. **203**, 739 (1979); J. D. Bohlin, in *Coronal Holes and High Speed Solar Wind Streams*, ed. J. B. Zirker (CoLorado Assoc. Univ. Press, Boulder, CO, 1977), p. 27.

[24] G. L. Withbroe, D. T. Jaffe, P. V. Foukal *et al.*, Astrophys. J. **203**, 528 (1976).

[25] G. L. Withbroe, Astrophys. J. **267**, 825 (1983).

[26] K. Wilhelm, E. Marsch, B. N. Dwivedi *et al.*, Astrophys. J. **500**, 1023 (1998).

[27] G. W. Pneuman and F. Q. Orrall, in *Physics of the Sun*, ed. P. A. Sturrock (Dordrecht: Reidel, 1986), Vol. II, p. 71; K. Shibata, in *Solar and Astrophysical Magnetohydrodynamic Flows*, ed. K. C. Tsinganos (Dordrecht:

kluwer, 1996), p. 217; J. H. Thomas, in *Solar and Astrophysical Magnetohydrodynamic Flows*, ed. K. C. Tsinganos (Dordrecht: kluwer, 1996), p. 39; K. Southwell, Nature **390**, 235 (1997).

[28] H. M. Olussei, A. B. C. Walker II, D. I. Santiago *et al.*, Astrophys. J. **527**, 992 (1999); H. M. Olussei, A. B. C. Walker II, J. Porter *et al.*, Astrophys. J. **524**, 1105 (1999).

[29] H. Tasso and G. N. Throumoulopoulos, Phys. Plasmas **5**, 2378 (1998).

[30] M. Furkawa, Y. Nakamura, S. Hamaguchi, and M. Wakatani, J. Plasma Fusion Res. **76**, 937 (2000).

[31] Z. Yoshida *et al.*, in *Non-Neutral Plasma Physics III* (American Institute of Physics, 1999) p. 397.

[32] O. A. Hurricane, Phys. Plasmas **5**, 2197, (1998).

[33] L. C. Steinhauer, Phys. Plasmas **6**, 2734, (1999).

[34] For simulation studies, see E. J. Charamana, R. A. Nebel, and D. D. Schnack, Phys. Fluids **26**, 1305, (1983); A. Y. Aydemir and D. C. Barnes, Phys. Rev. Lett. **52**, 930, (1984); T. Sato and K. Kusano,

ibid. **54**, 808, (1985); Z. Yoshida, K. Kusano, and N. Inoue, Phys. Fluids **30**, 2465, (1987)

[35] H. Grad and H. Rubin, in *Second United Nation Conference on the Peaceful Uses of Atomic Energy* (IAEA, Geneva, 1958), Vol. 31, p. 190-197.

[36] S. M. Mahajan and Z. Yoshida, Phys. Plasmas **7**, 635 (2000).

[37] In L. C. Steinhauer and A. Ishida, Phys. Rev. Lett. **79**, 3423, (1997), the double Beltrami equation has been derived by invoking a variational principle using h_1 and h_2 as rugged invariants; $\delta(E - \mu_1 h_1 - \mu_2 h_2) = 0$ directly leads (2.22) and (2.23) with $\mu_1 = -1/a$ and $\mu_2 = 1/b$.

[38] E. N. Parker, J. Grophys. Res., **97**, 4311 (1992).

[39] J. Birn, J. T. Gosling, M. Hesse, T. G. Forbes, and E. R. Priest, Astrophys. J. **541**, 1078 (2000).

[40] K. Kusano, Y. Suzuki, and K. Nishikawa, Apj. **441**, 942 (1995).

[41] K. Kusano and K. Nishikawa, Apj. **461**, 415 (1996).

[42] T. Sakurai, Solar Phys. **121**, 347 (1989).

[43] T. G. Forbes and P. A. Isenberg, Apj. **373**, 294 (1991).

[44] T. G. Forbes and E. R. Priest, Apj. **446**, 377 (1995).

[45] D. Biskamp, *Non-linear Magnetohydrodynamics* (Cambridge University Press, Cambridge, England, 1993), p.316.

[46] S. M. Mahajan, R. Miklaszewski, K. I. Nikol'skaya, and N. L. Shatashvili, arXiv. physics 0003086-September 27, 2000; preprint of ICTP IC/2000/31; Phys. Plasmas 2001 (accepted).

[47] E. N. Parker, Astrophys. J. **330**, 474 (1988).

[48] T. Tajima and K. Shibata, *Plasma Astrophysics*, (Addison-Wesley, Reading, Mass., 1989), p.210.

[49] A. J. Hundhausen, *Introduction to space physics*, ed. M. G. Kivelson and C. T. Russell (Cambridge University Press, Cambridge 1995), p.91.

[50] G. S. Choe and C. Z. Cheng, Astrophys. J. **541**, 449 (2000).

[51] M. J. Aschwanden, R. W. Nightingale, and D. Alexander, Astrophys. J. **541**, 1059 (2000).

[52] S. M. Mahajan, R. Miklaszewski, K. I. Nikol'skaya, and N. L. Shatashvili, Advaces in Space Research 2001 (accepted).

[53] Here we set $L = \sqrt{2}$. If we choose a large L, for example $\sqrt{2} \times 10^n$, multiplying h_1, h_2 and E by 10^{2n} will give the same result.

[54] S. D. Scott, P. H. Diamond *et al.*, Phys. Rev. Lett. **64**, 531 (1990).

[55] F. M. Levinton, R. E. Bell *et al.*, Phys. Rev. Lett. **80**, 4887 (1998).

[56] L. L. Lao, K. H. Burrel *et al.*, Phys. Plasmas **3**, 1951 (1996).

[57] R. L. Miller, F. L. Waelbroeck *et al.*, Phys. Rev. Lett. **2**, 3676 (1995).

[58] Z. Yoshida, Phys.Fluids B **1**, 1702 (1989).

[59] R. V. Polvin, Soviet. Phys. Uspekhi. **3**, 677 (1961).

[60] A. Jeffrey and T. Taniuti, *Non-linear wave propagation* (Academic. New York, 1964), p.125 and 214.

[61] L. D. Landau and E. M. Lifshitz, *Electrodynamics of continuous media* (Pergamon. Oxford. 1960), p.247.

Acknowledgments

I wish to thank Professor Zensho Yoshida for many fruitful discussions and suggestions. He suggested this problem and stimulated interest in it. Without his adequate guidance, it would be difficult to overcome many difficulties and complete this research. I am specially grateful for his continuing guidance and encouragement.

I wish to express my gratitude to Professor S. M. Mahajan for stimulating and helpful discussions, especially during the autumn college in ICTP and the US/Japan Workshop in Univ. Tokyo.

I would like to thank Prof. N. L. Shatashvili for her discussions and suggestions especially regarding solar corona. I also wish to thank to Mr. Tomoya Tatsuno and Dr. Masaru Furukawa for their suggestions on numerical analysis.

I am also grateful to Prof. Yuichi Ogawa for discussions and kindness, to Prof. Vazha Berezhinani for his enlightening comments and suggestions and

to Associate Prof. Haruhiko Himura for his encouragement.

I would like to thank Mr. Junji Morikawa and Dr. Hitoshi Nihei for their encouragement and kindness.

Thanks are due to my many colleagues with whom I have discussed many times. I am grateful to Dr. Francesco Volponi who introduce me to many topics (not only physics but also history, culture, jokes etc), to Dr. Shigeo Kondoh for his interesting (sometimes funny?) suggestions and kindness, to Mr. Atsusi Ito for his helpful suggestions, to Mr. Ryusuke Numata whose research stimulated me, to Miss Miroslava Savcović for her encouragement, to Mr. Chihiro Nakasima for his helpful suggestions and kindness. I'm also grateful to Mr. Daisaku Ozawa, Mr. Keita Yagi, Mr. Manabu Ohhashi and Mr. Haruhiko Saito who were helpful to me during this research.

研究発表

(i) 原著論文

(1) S. Ohsaki and Z. Yoshida, Phys. Plasmas **7**, 2404 (2000).

(2) Z. Yoshida, S. M. Mahajan, S. Ohsaki *et al.*, Phys. Plasmas **8**, (2001), (to be published).

(ii) 学会発表

(1) 大崎 秀一, 吉田 善章, Beltrami 磁場中のプラズマにおけるショック構造, 日本物理学会, 1999 年 9 月 （岩手大学）.

(2) 大崎 秀一, 吉田 善章, Beltrami 渦の重ね合わせの理論及びコロナモデルへの応用, 日本物理学会, 2000 年 3 月 （関西大学）.

(3) M. Iqbal, S. Ohsaki and Z. Yoshida, *Optimization of double Beltrami equilibrium with ultra high beta*, 日本物理学会, 2000 年 3 月 （関西大学）.

(4) 大崎 秀一, 吉田 善章, 高速流をもつプラズマの超高ベータ緩和状態 -トロイダル平衡 - , 日本物理学会, 2000 年 9 月 （新潟大学）.

(5) S. Ohsaki and Z. Yoshida, *Shock structure of Beltrami magnetic*

fields in plasmas, Autumn College on Plasma Physics, ICTP, Trieste, Italy (1999).

(6) 大崎 秀一, 吉田 善章, プラズマにおける Beltrami 磁場のショック構造, 「プラズマ科学の新しい展開」研究会, 1999 年 12 月 （核融合科学研究所）.

(7) 大崎 秀一, 吉田 善章, Beltrami 渦の重ね合わせの理論及びコロナモデルへの応用, 第 3 回核融合エネルギー連合講演会, 2000 年 6 月（中部大学）.